ENHANCED ASSESSMENT OF FLIGHT CAPABILITIES OF AIRCRAFT USING ASYMMETRIC ATTITUDE FLIGHT ENVELOPE

BY

Mohammed Abdul Muqeeth

A Thesis Presented to the

DEANSHIP OF GRADUATE STUDIES

KING FAHD UNIVERSITY OF PETROLEUM & MINERALS

DHAHRAN, SAUDI ARABIA

In Partial Fulfillment of the

Requirements for the Degree of

MASTER OF SCIENCE

In

AEROSPACE ENGINEERING

December 2018

KING FAHD UNIVERSITY OF PETROLEUM & MINERALS

DHAHRAN- 31261, SAUDI ARABIA

DEANSHIP OF GRADUATE STUDIES

This thesis, written by **Mohammed Abdul Muqeeth** under the direction of his thesis advisor and approved by his thesis committee, has been presented and accepted by the Dean of Graduate Studies, in partial fulfillment of the requirements for the degree of **MASTER OF SCIENCE IN AEROSPACE ENGINEERING.**

Dr. Ayman M. Abdallah
(Advisor)

Dr. Wael G. Abdelrahman
(Co-Advisor)

Dr. Ayman M. Abdallah
Department Chairman

Dr. Samir N. Mekid
(Member)

Dr. Salam A. Zummo
Dean of Graduate Studies

Dr. Salman H. Al-Fifi
(Member)

8/4/19

Date

Dr. Mohammed A. Ghazy
(Member)

This thesis is dedicated to my parents and family for their continuous support, prayers, and motivation throughout my life. Also, to my mentor Dr. Ayman for his inspiration, supervision and everlasting support.

ACKNOWLEDGMENTS

I would first like to thank my advisor and chairman Dr. Ayman M. Abdallah for his unrelenting support, dedication and encouragement throughout my Master's degree and for facilitating me at every stage by going above and beyond to provide all the resources I needed to accomplish my tasks.

I would also like to thank Dr. Wael Abdulrahman for his excellent counsel and support throughout my Bachelor's and Master's degrees. I also acknowledge Dr. Ahmed Al Garni, former chairman of AE department, for giving me a chance to study aerospace engineering at KFUPM as an undergraduate and a graduate.

I also express gratitude to my thesis committee members, Dr. Samir Mekid, Dr. Mohammed Ghazy and Dr. Salman Al fifi, for their participation. I feel honored to have your advice and evaluation.

I thank my peers Mr. Sultan Ghazzawi and Mr. Hamza Ahmed Mir for their advice, camaraderie, support, both emotional and technical, and, commiseration during hardship.

Additionally, I have gratitude towards the AE department staff and faculty, who have known me since the start of my academics, for all their help.

My everlasting gratitude to my parents, Mr. Mohammed Abdul Majeed and Mrs. Adila Banu for raising me, being my strongest supporters, motivators and the kindest people in my life. To my siblings Osama and Firdous, for their companionship, care and support all through my life, I thank you both.

I also have deep gratitude toward my friends and former peers Ahmed Abdulwahab, Omar El Ali, Mohamed Laradji, Anas Laoui, Mohammed Said Abdullah, Zakaria Bahlouli and Abdoullah Sqalli for their continuing kindness, camaraderie, spirit and support for the duration of my academic life at KFUPM.

TABLE OF CONTENTS

LIST OF TABLES

LIST OF FIGURES

LIST OF ABBREVIATIONS

$\boldsymbol{m}$	:	aircraft mass
$\boldsymbol{V_T},\ \boldsymbol{\bar{q}}$	:	total aircraft velocity magnitude, dynamic pressure
$\boldsymbol{\bar{b}, \bar{c}, \bar{S}}$	:	wing span, mean aerodynamic chord, reference area
$\boldsymbol{\alpha, \beta, \gamma}$	:	angle of attack, sideslip angle, flight path angle
$\boldsymbol{I_{xx}, I_{yy}, I_{zz}}$	:	moments of inertia about x, y and z axes respectively
$\boldsymbol{I_{xz}}$	:	product of inertia about x and y axes
$\boldsymbol{u_b, v_b, w_b}$	:	velocity components in x, y and z body axes respectively
$\boldsymbol{F_{X_b}, F_{Y_b}, F_{Z_b}}$	:	forces along x, y and z body axes respectively
$\boldsymbol{L_b, M_b, N_b}$	:	moments about x, y and z body axes respectively
$\boldsymbol{p_b, q_b, r_b}$	:	angular rates about x, y and z body axes respectively
$\boldsymbol{T}$	:	total engine thrust
$\boldsymbol{C_*}$	:	total aerodynamic force and moments coefficients, where $*$ denotes X, Y, Z, L, M, N
$\boldsymbol{C_{a_b}}$	:	aerodynamic derivative for the effect of 'b' on 'a'
$\boldsymbol{C_{Lift}}$, $\boldsymbol{C_{Drag}}$	:	total aerodynamic lift and drag coeffcients
$\boldsymbol{x_s, u_s, f_d}$	:	flight state, control and state derivative vectors respectively
$\boldsymbol{J_d}$	:	trim objective/cost

ABSTRACT

Full Name : Mohammed Abdul Muqeeth

Thesis Title : Enhanced Assessment of Flight Capabilities of Aircraft using Asymmetric Attitude Flight Envelope

Major Field : Aerospace Engineering

Date of Degree : December 2018

An aircraft's flight envelope is used to define and study its various operating limits and flight regimes. However, typical flight envelopes, like the altitude vs. speed envelope, only represent flight at symmetric (ideal) aircraft attitudes and do not describe flight at asymmetric attitudes where sideslip and bank angles may be present. Hence, to expand on aircraft performance assessment, in this work, a non-traditional asymmetric attitude flight envelope is developed for mathematical models of a military and a business jet. This envelope, also called the angle of attack vs. sideslip or α-β envelope, is a bounded curve that describes the full extent to which an aircraft can be flown at asymmetric attitudes while trimmed (steady-state). The α-β envelope is comprised of trim points developed by optimizing the dynamics of an aircraft model while subject to constraints of aircraft control limitations and structural integrity. These trim points show the complete trim profile of the aircraft and hence describe the boundary of the asymmetric attitude flight envelope. Following envelope development, the observed flight operating limitations and peculiarities of both aircraft models are discussed. The envelope data revealed important

insights, which were previously not available, into performance requirements in terms of flight conditions and control surfaces. Further, the data also provided operating limitations due to factors like the control surfaces, propulsion unit, aerodynamic capability and structural integrity at the extremes of the aircrafts' capabilities. The results also showed a fundamental difference between the asymmetric trim capabilities of both aircraft models across their respective envelopes. Lastly, the flight performance information within this type of flight envelope has applications in the areas of designing flight control systems, which are highlighted.

ملخص الرسالة

الاسم الكامل: محمد عبد المغيث

عنوان الرسالة: تقييم مُحسَّن لقدرات الطيران للطائرات باستخدام غلاف وضعية طيران غير متماثل

التخصص: هندسة الطيران والفضاء

تاريخ الدرجة العلمية: : ديسمبر 2018 م

يستخدم غلاف طيران الطائرة لتحديد ودراسة حدود التشغيل في أنظمة الطيران المختلفة. ومع ذلك ، فإن أغلفة الطيران التقليدية ، مثل غلاف الارتفاع مقابل السرعة ، تمثل فقط الطيران في مواقف الطائرات المتماثلة (النموذجية) ولا تصف الطيران في المواقف غير المتماثلة التي قد توجد فيها زوايا الانزلاق والميل الجانبي. وبالتالي ، للتوسع في تقييم أداء الطائرات بشكل كامل ، في هذا العمل ، تم تطوير غلاف طيران غير متماثل ذي وضعية طيران غير متماثلة لطائرتين ذواتي قدرات مختلفة الأول نموذج لطائرة عسكرية والثاني لطائرة رجال أعمال. هذا المغلف ، والذي يُطلق عليه أيضًا غلاف زاوية الهجوم في مقابل زاوية الانزلاق α-β ، هو منحنى مُحدّد يصف المدى الكامل لقابلية تحقيق توازن الطائرة في وضعيات أثناء الطيران في الحالة المستقرة. يتكون غلاف α-β من مجموعة نقاط الحالات المستقرة التي تم تطويرها وايجادها من خلال طرق الحل الأمثل لديناميكيات طراز الطائرة مع مراعاة قيود التحكم في الطائرة والسلامة الهيكلية. توضح مجموعة النقاط الحالات المستقرة الكامل للطائرة في وضعية طيران غير متماثلة ، وتصف حدود غلاف لوضعية الطيران غير المتماثلة. بعد تطوير الغلاف ، تتم مناقشة القيود المفروضة على تشغيل الطيران وخصائص كلا الطرازين. كشفت بيانات الغلاف عن رؤى مهمة لم تكن متوفرة في السابق فيما يتعلق بمتطلبات الأداء من حيث ظروف الطيران وأسطح التحكم. علاوة على ذلك ، قدمت البيانات أيضًا قيودًا على التشغيل نظرًا لعوامل عدة مهمة مثل أسطح التحكم ووحدة الدفع والقدرة

الديناميكية الهوائية والسلامة الهيكلية عند أقصى درجات قدرات الطائرات. أظهرت النتائج أيضًا اختلافًا جوهريًا بين إمكانات الحالات المستقرة غير المتماثلة لكلا الطرازين عبر الغلافين المعنيين. أخيرًا ، يقدم الغلاف أيضاً معلومات أداء الرحلة ضمن هذا النوع من مظاريف الطيران تطبيقات في مجالات تصميم أنظمة التحكم في الطيران ، والتي يتم تسليط الضوء عليها.

CHAPTER 1

RESEARCH DESCRIPTION

1.1 Introduction

1.1.1 Background

Flight envelopes have been utilized in aviation for aircraft design and development. There are several categories of flight envelopes corresponding to different types of aircraft operating limits. The typical speed-altitude envelope, for instance, shows the range of speed limits with respect to flight altitude in which that aircraft can operate safely.

Figure 1 (top figure) shows the traditional speed-altitude envelope for three classes of aircraft including a supersonic fighter aircraft and a subsonic commercial jet. Figure 1 also (bottom figure) indicates typical types of limiting bounding regions encountered at different regimes of flight. The bounded region of the envelope, for each aircraft, defines the flight conditions that are safe for flight for each respective aircraft. Present on the envelopes are various aircraft operating limits. Towards the low-speed region of the envelopes, for example, is the minimum speed boundary, which occurs as a result of the aerodynamic stall phenomenon.

Also, at the top of the envelopes are the altitude ceilings for the aircraft. For the military jet, the ceiling is mainly due to its maximum engine thrust capability whereas the ceiling for the commercial jet arises from the cabin pressure limitations prescribed by the aviation regulatory authorities.

At the high-speed boundary, are two operating limits; one from the airframe structural load limitations, and the other (at higher altitudes) from the maximum engine capability. The structural load limit is due to the maximum dynamic pressure limit, which dictates the highest speed that the aircraft can fly at without (aerodynamically) overloading the airframe. Exceeding this speed can cause damage to the aircraft body, and, can also lead to wing flutter which is a dangerous oscillation of the wing structure causing potential break-up of the airframe. The maximum engine limitation at the high-speed boundary is due to the maximum speed that can be attained when the engine is producing maximum thrust. In supersonic aircraft, exceeding this speed can cause formation of shock waves at the intake duct of the engine and can lead to malfunction of the engine unit [7],[10],[14].

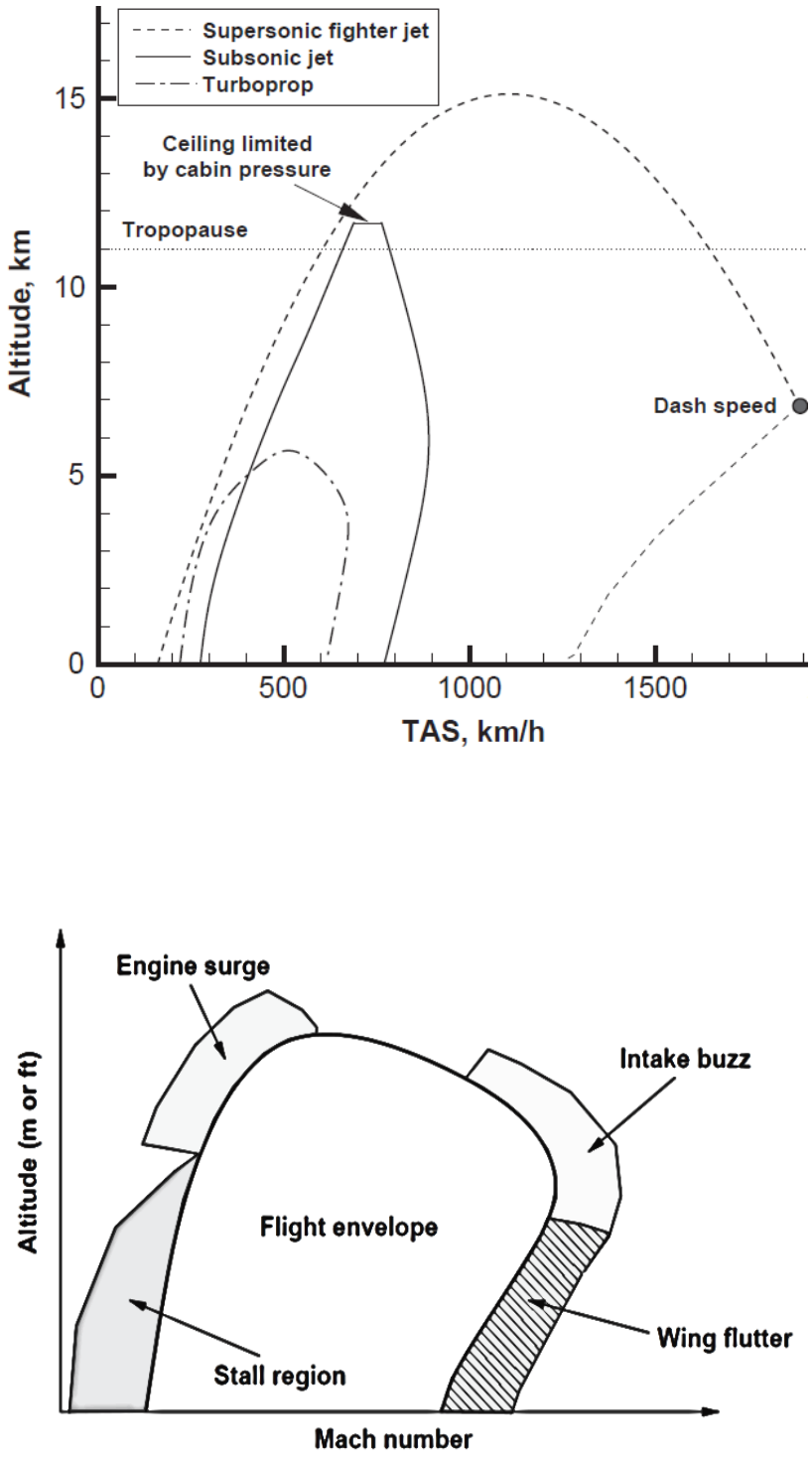

Figure 1: (Top) Speed-Altitude Flight Envelope for Three Aircraft Classes [7]; (Bottom) General Representation of Speed-Altitude Envelope [7]

The speed-altitude envelopes for both supersonic and subsonic aircraft show the same types of limits at the envelope boundary, however, the range of speed and altitude limits for both aircrafts are different, as expected, since their design objectives and characteristics are not the same, which cause the performance limits of the military and commercial aircraft to differ. The military jet is supersonic-capable, whereas the business jet has maximum operating speeds in the high subsonic range. The altitude ceilings are also much higher for the military jet, while the business jet has a much lower operating ceiling, which is typical of aircraft in its class [7],[15].

Another type of common flight envelope is the Load factor vs. speed or V-n envelope as shown in Figure 2. This envelope shows the operating structural load limitations in terms of the load factor (n) experienced by an aircraft (which is the aircraft lift to weight ratio), as a function of speed (V). For an aircraft with fixed mass, the total lift, and therefore the aerodynamic load on the aircraft, varies with flight operating conditions like altitude, maneuver (pull up/down), aircraft configuration, etc. The profile of the V-n curve is unique to the aircraft being investigated and the aircraft has to be operated within the bounds of the envelope for safe flight, and outside the envelope, the aircraft will experience structural overloading and may get severely damaged. The left-most positive and negative load factor curves are the stall curves, and these show the maximum achievable load factor for the aircraft at stall conditions. These curves flatten at the ultimate positive and negative load limit lines, which are pre-specified structural limits by the manufacturer. The right-side line is the structural limit from the maximum dynamic pressure and corresponds to the highest speed that the aircraft can be safely flown at, which is also manufacturer-specified. This envelope is therefore crucial to understand for

test pilots, design engineers as well as operators of the aircraft so that the maximum combinations of load factor and airspeeds are well known and never exceeded during flight [4],[5].

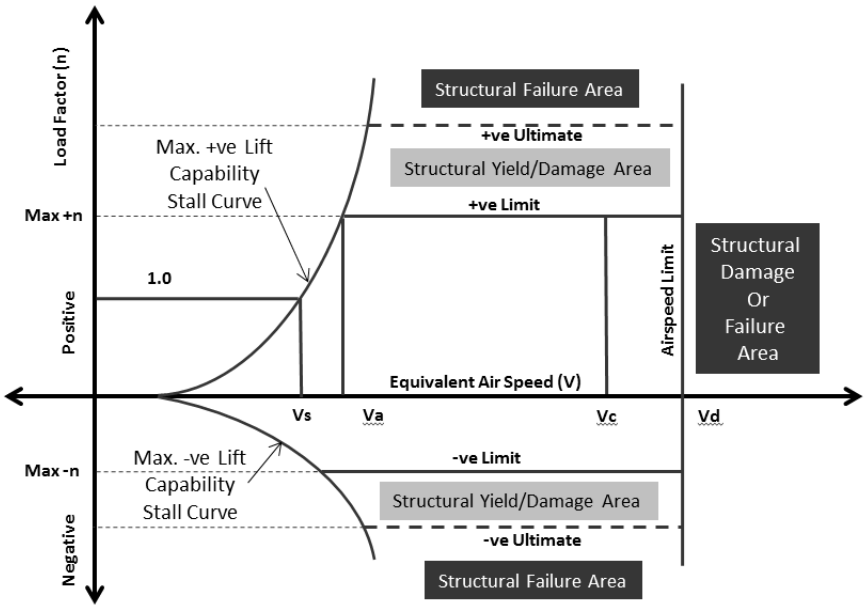

Figure 2: General Representation of Load Factor vs. Speed (V-n) Envelope [4]

Analyzing the information in flight envelopes such as Figure 1 and Figure 2 is imperative to understand the safe flight operating conditions and to prevent any loss of control of the aircraft. Additionally, flight envelopes can give pilots enhanced situational awareness regarding aircraft responses to different conditions and configurations. Also, analyzing the data used in envelope development can provide a multitude of performance and technical insights which can be utilized in the development of aircraft control systems [9].

Hence, these flight envelopes are a crucial tool for engineers. However, all the data in these envelopes correspond to a symmetric flight attitude where the wings are level with the horizon, and no lateral asymmetric flight is involved. Confining the aircraft to this attitude not only offers a limited view of aircraft performance, but this is also a very idealistic case of flight since the aircraft is often forced to adopt asymmetric orientations. Performance in general is affected by the change in lateral attitude of an aircraft, and knowing the exact extent of the effect of asymmetric attitudes is important in completing the aircraft performance view. Asymmetries in attitude can arise during flight for several reasons such as - broken components on wings, failure of one of the landing gears to deploy, sideslip from crosswinds or gusts, turbulence, control surfaces hardovers, etc. The asymmetry can also be deliberate such as while maneuvering or turning or in uncoordinated flight [1],[2],[14].

To analyze complete aircraft performance limits, including operability at asymmetric attitudes, a non-conventional flight envelope called the **angle of attack vs. sideslip angle** or **α-β envelope** is developed in this work. In this envelope, the lateral motion variables are present and considered, and, their effect on aircraft motion and performance is also determined. This lateral motion inclusion is represented on the envelope by the sideslip angle on the horizontal axis. Hence this envelope extends the scope, of the traditional envelopes and can be used for enhanced assessment of flight performance of aircraft. This flight envelope defines the extent to which an aircraft can perform rectilinear flight while having asymmetric aerodynamic attitudes i.e. a horizontal slipping flight condition [1],[2].

Understanding the behavior of fundamental flight characteristics at asymmetric attitudes is crucial at different design stages of an aircraft. This envelope is a relatively new and intriguing way to examine an aircraft's dynamics and understand its performance weaknesses and strengths. The results obtained can be utilized in many fields like aircraft control system design and others.

1.1.2 Aircraft Models

In this work, two aircraft models are used corresponding to different design operating missions and performance capabilities. However, the same core methodology will be applied to both models to obtain results. This also provides an opportunity to contrast the performance features and overall behavior of the two aircraft in various flight conditions. These aircraft models are:

(i) The Reduced Order F-16 aerodynamic model. The F-16 aircraft (shown in Figure 3) is a modern military jet known for its high agility and maneuverability [11],[14].

(ii) The high performance subsonic generic executive jet model with T-tail configuration (shown in Figure 4) [13].

Both models are six degree-of-freedom nonlinear models, and reasonably equivalent to each other in terms of sophistication and complexity. The mathematical representation of these models along with their components are detailed in a subsequent chapter.

Figure 3: F-16 Military Aircraft [6]

Figure 4: Small Executive Jet with T-tail [5]

1.2 Literature Review

In current literature, there is a severe dearth of research regarding the modeling of asymmetric attitude flight and the study of the full lateral aspect of flight performance. Due to this reason, the literature available that describes and develops the asymmetric attitude flight envelope is very scarce. Presented below are the literature that introduced the concept of analyzing asymmetric attitude flight performance using the $\alpha - \beta$ envelope**.**

Abdallah, Newman and Omran [1],[2] first introduced the notion of the asymmetric attitude flight envelope as an angle of attack (α) vs. sideslip angle (β) region. The bounded portion of this envelope depicts the asymmetric trimmability extent of an aircraft in terms of the range of angles of attack and sideslips angles in which an aircraft is capable of trimmed flight. In other words, it shows all possible attitudes (orientations) that an aircraft can adopt while maintaining rectilinear equilibrium flight. The boundary of the envelope is determined by several factors which are - aerodynamics, control and engine capabilities, and structural aspects of the specific aircraft being examined.

Each point inside the envelope is a (β, α) ordered couple, and represents an attitude at which the aircraft is capable of trimmed flight. The boundary of the envelope is reached when the aircraft encounters a (β, α) pair at which trimmed (steady) flight is beyond the capability of that aircraft being investigated. This envelope is developed for a fixed altitude since the asymmetric attitude performance of an aircraft varies with altitude. In this case, the altitude is at sea level [1],[2].

Reference [3] by Abdallah adds the altitude perspective by developing the asymmetric attitude envelope for a supersonic, high agility jet model over its entire operating altitude range resulting in a 3D surface describing the asymmetric trimmability extent of an aircraft in terms of the range of angles of attack and sideslips angles, and altitude. It is seen that the envelope size, and therefore the asymmetric trimmability, reduces as the aircraft rises in altitude. The same aerodynamics, control, engine, and structural factors were considered for this 3D envelope's boundary.

References [9] and [16] highlight the significance and utility of the development of the complete trim profile of an aircraft. All modern aircraft have fly-by-wire systems and flight control computers, which essentially fly the aircraft in the desired path and manner by performing real-time stability and trim state calculations. Many of these systems use a database approach where an offline database of trim envelope data, atmospheric data and modeling of common structural, system and engine failure responses is used to append the functionality of online systems by providing them with a ready repository of flight data to compute from. The advantage over other systems is that this approach is far more efficient and faster because instead of solving a myriad of complicated equations and flight parameters in real-time, the system can select a flight scenario closest to the actual one from the database onboard and interpolate to replicate the exact flight condition experienced. Then, the required flight parameters can be easily computed using this data and the aircraft can react accordingly. Figure 5 illustrates a flight control system that uses an offline database of various types flight envelope data and flight conditions to support the online flight control computers.

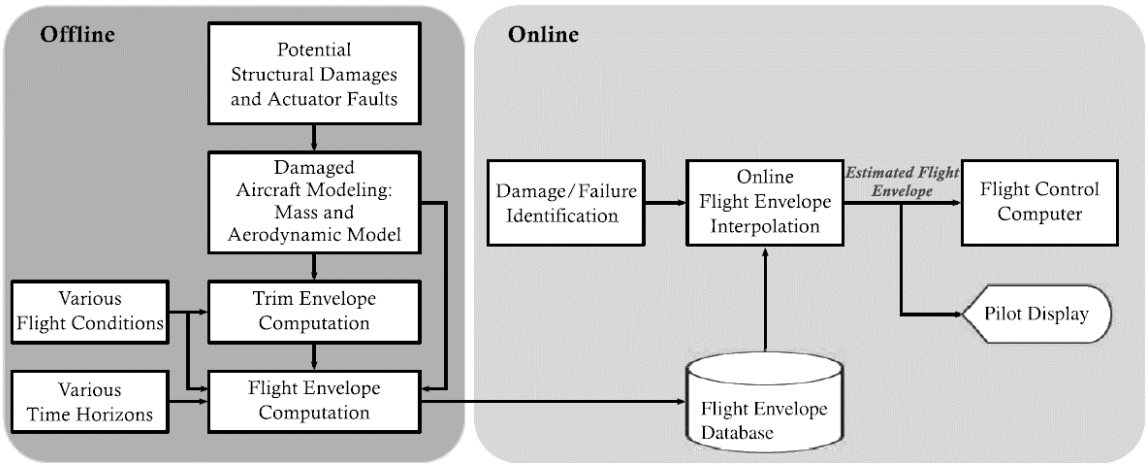

Figure 5: Flight Control Scheme using (offline) Trim Envelope Database [9]

Reference [9] additionally states the utility of this approach not only for an aircraft operating normally, but also for a scenario where the aircraft experiences asymmetric damage, like airframe damage or engine failure on one side of the aircraft, since this type of damage modeling is very uncommon in literature and requires readjusting the initial model properties and may introduce additional interaction between properties, like inertial coupling. The work done in this thesis addresses the issue of understanding asymmetric operability of aircraft, and can also be used compute trim envelopes corresponding to any flight scenario.

1.3 Motivation

The complete performance perspective of an aircraft can only be obtained if both the longitudinal and lateral extremes of flight are well known. The conventional flight envelopes and current literature do not include the lateral view of aircraft performance. Therefore, asymmetric flight conditions are not fully being investigated. Hence, the development of a methodology to develop the asymmetric attitude flight envelope is

carried out in this work. Additionally, this asymmetric attitude envelope also addresses the aspects of performance missing in other envelopes like – description of flight in the stall and post-stall domain, control power authority across the operating envelope, and, the trimmability-controllability relationship at any aircraft orientation [1],[2].

The developed performance data from the asymmetric attitude flight envelope, can also enable development or improvement of robust flight stability and maneuverability control systems by integrating the full aircraft trim performance data into the offline database segment of any type of flight control system. Additionally, the algorithm developed in this work can also model trim performance data for a damaged aircraft by adjusting the initial conditions and aircraft (geometric/mass/inertial) properties to simulate any damage or component failure within the aircraft, and subsequently compute performance data corresponding to the damaged flight condition [1],[2],[9],[16].

Also, this work applies this concept of asymmetric flight envelope on two aircraft models differing in terms of operating missions and performance capabilities which provides an opportunity to compare the performance limits in various flight conditions. The information from the envelope provides deep insights into flight capability and limitations with respect to the two aircraft models used. Further, it reveals details about aircraft operation and control limitations that were previously not readily noticeable.

1.4 Thesis Objectives

(i) Develop the asymmetric attitude flight envelope for the military jet model

(ii) Develop the asymmetric attitude flight envelope for the business jet model

(iii) Analyze the resulting envelope profiles and study the performance requirements and limits for both aircraft models.

(iv) Present the important performance insights and contrast the major differences between the two aircraft models, and, identify the applications of the results with respect to enhanced flight performance assessment and control.

1.5 Learning Outcomes

This work relies on accurately developing the **α-β** flight envelope for both flight models. Accordingly, the major learning outcomes are –

(i) To understanding the nature of asymmetric trimmed flight characteristics for two aircraft models integrating dynamics, aerodynamic and propulsive characteristics

(ii) To fully comprehend the theory behind the envelope development process, and the requirements and methodology employed therein

(iii) To set up the models, numerically compute and develop the **α-β** flight envelopes in a systematic approach while documenting the various pitfalls encountered.

Envelope development is the key outcome in terms of learning and skill development in this work. This process is very sensitive to the different operating flight conditions encountered. This necessitates numerous successive iterations of fine tuning the optimization algorithm developed in this work. This recursion led to an exhaustive process until the final envelope profile was developed as required. The source models were also modified to account accurately for lateral parameters.

1.6 Thesis Outline

The outline of this thesis is as follows. Chapter 1 presents the background and the main motivation behind this work, along with brief description of the models used, and, the objectives and expected outcomes of this work.

Chapter 2 explores the mathematical formulation of the dynamics of flight by stating and describing the governing equations of motion used to describe the six degree-of-freedom motion of an aircraft in three-dimensional space. Chapter 3 details the two aircraft models used in this work, corresponding to a military jet and a business jet model, as mentioned earlier. In Chapter 4, certain discrepancies which were present in the aerodynamic model data of the military jet are explained and appropriately corrected to ensure accuracy of the results required.

This is followed by Chapter 5 which explains the methodology by which the envelope is obtained through development of trim points in both aircraft models via optimization of the dynamics of the aircraft models while considering all constraints of aircraft control surface limits, propulsion limits and structural load limits, to obtain the extreme asymmetric variations for flight conditions represented here in terms of α and β angles on the envelope .

Chapter 6 shows the results and discussion where the obtained results in terms of the α-β envelopes for both aircraft models are presented, and the observations regarding the aircraft performance at asymmetric attitudes are remarked upon. Also, the potential applications of such envelope development methodology and the performance data within the α-β envelopes are highlighted. Finally, the conclusion in Chapter 7 of the work is described, and the selected results are reiterated along with comments and recommendations.

CHAPTER 2

DYNAMICS OF FLIGHT

The motion of the aircraft can be well described by Newton's laws of motion derived in a body referenced frame or coordinate system. In deriving the equations of motion of an aircraft, several assumptions are made, such as non-rotating flat Earth, rigid body airframe, no actuator dynamics, and constant mass vehicle. The flat Earth assumption is equivalent to assuming that the Earth is an inertial-frame. The derivation of the equations of motion starts with Newton's laws of motion being applied to a system of particles bounding the rigid body aircraft. Six governing kinetic equations that describe the six degree of freedom (DoF) motion exist for three translational velocities (u,v,w) and three angular velocities (p,q,r). Six governing kinematic equations also exist for three translational inertial positions (X,Y,Z) and three angles of roll, pitch and yaw respectively (ϕ,θ,ψ), which are also known as the Euler angles. [1],[2].

2.1 Body Reference Frame

Here a body-referenced frame or coordinate system is used which is fixed to the center of gravity of the aircraft. This frame moves and rotates with the aircraft and hence is a non-inertial frame. Newton's laws, which are used to derive the aircraft equations of motion, are valid only in an inertial frame. Hence an inertial frame that does not experience any rotation or acceleration is defined here as a coordinate system fixed on a point on the Earth. The translational and rotational motion of the aircraft can be tracked using this inertial Earth fixed reference. This inertial and body-fixed reference coordinate system is shown in Figure 6. It is also necessary to define the angle of attack α and sideslip angle β which show the orientation of the body force and moments acting on the aircraft relative to the total aircraft velocity vector ($\boldsymbol{V}$). Figure 6 also shows these two aerodynamic angles in addition to the description of the aircraft body, and wind axes.

The α and β angles can be described mathematically in terms of the total aircraft velocity and its body components as –

$$\alpha = tan^{-1}\frac{w_b}{u_b} \tag{1}$$

$$\beta = sin^{-1}\frac{v_b}{V_T} \tag{2}$$

Where, $V_T = \sqrt{u_b^2 + v_b^2 + w_b^2}$

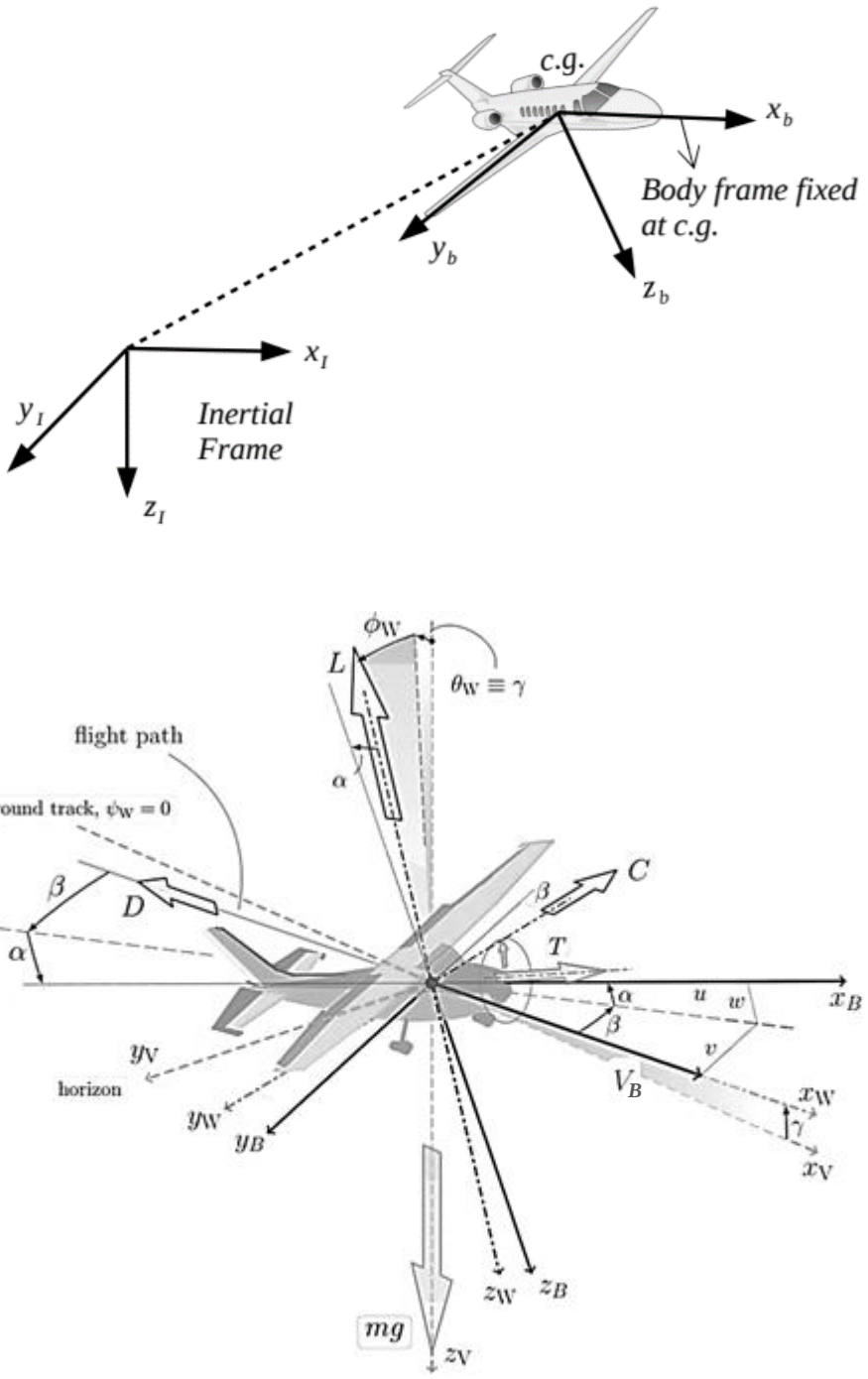

Figure 6: Body and Inertial axes system (top) [12]; Description of Body Frame Axes with α and β (bottom) [8]

The transformation among the axes of inertial, body, and wind frames is done through rotation of these axes relative to each other. The two relevant transformation relations in this work, which are transformation from wind-to-body axes and body-to-inertial axes, are given here in the form of their respective transformation (direction cosine) matrices [13].

The wind-to-body axes transformation and vice versa are given below and involve rotation through the angle of attack and sideslip angles -

$$C_{b/w} = \begin{bmatrix} \cos\alpha\cos\beta & -\cos\alpha\sin\beta & -\sin\alpha \\ \sin\beta & \cos\beta & 0 \\ \sin\alpha\cos\beta & -\sin\alpha\sin\beta & \cos\alpha \end{bmatrix} \tag{3}$$

$$C_{w/b} = C_{b/w}^{T}$$

The transformation from body-to-inertial axes involves a sequence of three planar rotations through the Euler angles of yaw, pitch and roll (ϕ, θ, ψ) and the transformation matrix after rotation is given below -

$$C_{I/b} =$$

$$\begin{bmatrix} \cos\theta\cos\psi & -\cos\phi\sin\psi + \sin\phi\sin\theta\cos\psi & \sin\phi\sin\psi + \cos\phi\sin\theta\cos\psi \\ \cos\theta\sin\psi & \cos\phi\cos\psi + \sin\phi\sin\theta\sin\psi & -\sin\phi\cos\psi + \cos\phi\sin\theta\sin\psi \\ -\sin\theta & \sin\phi\cos\theta & \cos\phi\cos\theta \end{bmatrix} \tag{4}$$

$$C_{b/I} = C_{I/b}^{T}$$

2.2 Aircraft Equations of Motion for Body Referenced Frame

As mentioned earlier, these equations that completely describe the six DoF motion of a rigid body in 3D space, are derived using Newton's laws of motion. The assumptions made are a non-rotating flat Earth, rigid body airframe, no actuator dynamics, and constant mass vehicle. The six kinetic equations that yield the linear and angular accelerations are derived first using the Newton linear and angular momentum equations in the inertial frame. However, it is more convenient to write these equations in the body referenced frame utilizing the vector derivative transformation relationship. This relationship is described as follows –

$$\left(\frac{d[\boldsymbol{vector}]}{dt}\right)_I = \left(\frac{d[\boldsymbol{vector}]}{dt}\right)_a + \boldsymbol{\omega}_a \times [\boldsymbol{vector}]$$

Where $\boldsymbol{\omega}_a$ is the angular velocity vector that describes the angular rotation between the two frames *a* and *I*.

The linear momentum equation is thus written in the body referenced frame as – [1]

$$\sum \boldsymbol{F}_b = m\left(\dot{\boldsymbol{V}}_b + \Omega \boldsymbol{V}_b\right) \tag{5}$$

Where,

$$\sum \boldsymbol{F}_b = \begin{Bmatrix} F_{x,b} \\ F_{y,b} \\ F_{z,b} \end{Bmatrix} + C_{b/I} m\boldsymbol{g}; \qquad \boldsymbol{g} = \begin{Bmatrix} 0 \\ 0 \\ g \end{Bmatrix}; \qquad \boldsymbol{V}_b = \begin{Bmatrix} u_b \\ v_b \\ w_b \end{Bmatrix}; \qquad \Omega = \begin{bmatrix} 0 & -r_b & q_b \\ r_b & 0 & -p_b \\ -q_b & p_b & 0 \end{bmatrix}$$

Equation (5) is then written in terms of the body translational accelerations as -

$$\dot{\boldsymbol{V}}_b = -\Omega \boldsymbol{V}_b + \frac{1}{m}\sum \boldsymbol{F}_b \tag{6}$$

Upon substitution and expansion, the body accelerations are obtained as -

$$\dot{u}_b = r_b v_b - q_b w_b - g\,sin\,\theta + \frac{1}{m}(F_{X_b} + T) \tag{7}$$

$$\dot{v}_b = -r_b u_b + p_b w_b + g\,sin\,\phi\,cos\,\theta + \frac{1}{m}F_{Y_b} \tag{8}$$

$$\dot{w}_b = q_b u_b - p_b v_b + g\,cos\,\phi\,cos\,\theta + \frac{1}{m}F_{Z_b} \tag{9}$$

Similarly, the next three kinetic equations which provide the angular accelerations are derived from the Newton angular momentum equation written in the body referenced frame as shown below – [1]

$$\sum \boldsymbol{M}_b = J\dot{\boldsymbol{\omega}} + \Omega J\boldsymbol{\omega} \tag{10}$$

In terms of the angular acceleration, the above equation is written as –

$$\dot{\boldsymbol{\omega}} = J^{-1}(-\Omega J\boldsymbol{\omega} + \sum \boldsymbol{M}_b) \tag{11}$$

Where,

$$\sum \boldsymbol{M}_b = \begin{Bmatrix} L_b \\ M_b \\ N_b \end{Bmatrix}; \qquad \boldsymbol{\omega} = \begin{Bmatrix} p \\ q \\ r \end{Bmatrix};$$

$$J = \begin{bmatrix} I_{xx}^b & -I_{xy}^b & -I_{xz}^b \\ -I_{xy}^b & I_{yy}^b & -I_{yz}^b \\ -I_{xz}^b & -I_{yz}^b & I_{zz}^b \end{bmatrix}$$

$$J^{-1} = \frac{1}{\Delta}\begin{bmatrix} I_{yy}^b I_{zz}^b - \left(I_{yz}^b\right)^2 & I_{yz}^b I_{xz}^b + I_{xy}^b I_{zz}^b & I_{xy}^b I_{yz}^b + I_{xz}^b I_{yy}^b \\ I_{yz}^b I_{xz}^b + I_{xy}^b I_{zz}^b & I_{zz}^b I_{xx}^b - (I_{xz}^b)^2 & I_{xy}^b I_{xz}^b + I_{yz}^b I_{xx}^b \\ I_{xy}^b I_{yz}^b + I_{xz}^b I_{yy}^b & I_{xy}^b I_{xz}^b + I_{yz}^b I_{xx}^b & I_{xx}^b I_{yy}^b - \left(I_{xy}^b\right)^2 \end{bmatrix} = \frac{1}{\Delta}\begin{bmatrix} k_1^b & k_2^b & k_3^b \\ k_2^b & k_4^b & k_5^b \\ k_3^b & k_5^b & k_6^b \end{bmatrix}$$

$$\Delta^b = I_{xx}^b I_{yy}^b I_{zz}^b - 2I_{xy}^b I_{yz}^b I_{xz}^b - I_{xx}^b\left(I_{yz}^b\right)^2 - I_{yy}^b (I_{xz}^b)^2 - I_{zz}^b\left(I_{xy}^b\right)^2$$

Substituting the vector and matrix components and expanding yields the body angular accelerations –

$$\begin{aligned} \dot{p}_b = \frac{1}{\Delta^b}\Big[& k_1^b\left\{\left(I_{yy}^b - I_{zz}^b\right)q_b r_b + I_{yz}^b(q_b^2 - r_b^2) + \left(I_{xz}^b q_b - I_{xy}^b r_b\right)p_b + L_b\right\} \\ & + k_2^b\left\{(I_{zz}^b - I_{xx}^b)p_b r_b + I_{xz}^b(r_b^2 - p_b^2) + \left(I_{xy}^b r_b - I_{yz}^b p_b\right)q_b + M_b\right\} \\ & + k_3^b\left\{\left(I_{xx}^b - I_{yy}^b\right)p_b q_b + I_{xy}^b(p_b^2 - q_b^2) + \left(I_{yz}^b p_b - I_{xz}^b q_b\right)r_b + N_b\right\}\Big] \end{aligned} \tag{12}$$

$$\dot{q}_b = \frac{1}{\Delta^b}\left[k_2^b\left\{\left(I_{yy}^b - I_{zz}^b\right)q_b r_b + I_{yz}^b\left(q_b^2 - r_b^2\right) + \left(I_{xz}^b q_b - I_{xy}^b r_b\right)p_b + L_b\right\}\right.$$
$$+ k_4^b\left\{\left(I_{zz}^b - I_{xx}^b\right)p_b r_b + I_{xz}^b\left(r_b^2 - p_b^2\right) + \left(I_{xy}^b r_b - I_{yz}^b p_b\right)q_b + M_b\right\} \quad (13)$$
$$\left. + k_5^b\left\{\left(I_{xx}^b - I_{yy}^b\right)p_b q_b + I_{xy}^b\left(p_b^2 - q_b^2\right) + \left(I_{yz}^b p_b - I_{xz}^b q_b\right)r_b + N_b\right\}\right]$$

$$\dot{r}_b = \frac{1}{\Delta^b}\left[k_3^b\left\{\left(I_{yy}^b - I_{zz}^b\right)q_b r_b + I_{yz}^b\left(q_b^2 - r_b^2\right) + \left(I_{xz}^b q_b - I_{xy}^b r_b\right)p_b + L_b\right\}\right.$$
$$+ k_5^b\left\{\left(I_{zz}^b - I_{xx}^b\right)p_b r_b + I_{xz}^b\left(r_b^2 - p_b^2\right) + \left(I_{xy}^b r_b - I_{yz}^b p_b\right)q_b + M_b\right\} \quad (14)$$
$$\left. + k_6^b\left\{\left(I_{xx}^b - I_{yy}^b\right)p_b q_b + I_{xy}^b\left(p_b^2 - q_b^2\right) + \left(I_{yz}^b p_b - I_{xz}^b q_b\right)r_b + N_b\right\}\right]$$

The next six kinematic equations of motion are the Euler angle rates and the inertial velocities. The orientation of an aircraft can be described by the Euler angles rotations relative to the inertial Earth frame axes. The Euler angle rates are resolved into components relative to body referenced angular rates and expressed below as – [1]

$$\dot{\phi} = p_b + (tan\,\theta\, sin\,\phi)q_b + (tan\,\theta\, cos\,\phi)r_b \quad (15)$$

$$\dot{\theta} = (cos\,\phi)q_b - (sin\,\phi)r_b \quad (16)$$

$$\dot{\psi} = (sin\,\phi/cos\,\theta)q_b + (cos\,\phi/cos\,\theta)r_b \quad (17)$$

The inertial velocity equations are obtained by transforming the body velocities to their inertial counterparts through the appropriate transformation matrix. The resulting equations are given below – [1]

$$\dot{X} = (cos\,\theta\,cos\,\psi)u_b + (-cos\,\phi\,sin\,\psi + sin\,\phi_b\,sin\,\theta\,cos\,\psi)v_b + (sin\,\phi\,sin\,\psi + cos\,\phi\,sin\,\theta\,cos\,\psi)w_b \quad (18)$$

$$\dot{Y} = (cos\,\theta\,sin\,\psi)u_b + (cos\,\phi\,cos\,\psi + sin\,\phi\,sin\,\theta\,sin\,\psi)v_b + (-sin\,\phi\,cos\,\psi + cos\,\phi\,sin\,\theta\,sin\,\psi)w_b \quad (19)$$

$$\dot{Z} = (-sin\,\theta)u_b + (sin\,\phi\,cos\,\theta)v_b + (cos\,\phi\,cos\,\theta)w_b \quad (20)$$

These equations of motion describe fully the motion of an aircraft. These equations have been written such that the 12 aircraft state derivatives (like $\dot{u}, \dot{X}, etc.$) are each expressed in terms of their respective inputs. The equations in this form are conducive to programmable computation and are used for calculation of trim (equilibrium) flight requirements for any given initial condition of flight with asymmetric attitude (discussed in Chapter 5).

CHAPTER 3

Aircraft Models

3.1 F-16 Reduced Order Aircraft Model

This aerodynamics and propulsion model is used for the six DoF nonlinear simulation of an F-16 fighter aircraft. This model utilizes experimental data from a NASA wind tunnel study [11]. However, the model has been adapted in [14] and simplified the coefficient data as well as the engine model to reduce the order of complexity of the model and enable easier usability and understanding of the model properties. The reduced order model also enables better trim calculation and the effect of each individual parameter can be observed in an easier manner.

The aircraft model consists of the following components -

- **Aerodynamic Model** which contains data tables with aerodynamic coefficient data for an α range of $-10°$ to $+45°$ and a β range of $-30°$ to $+30°$. This data is used to determine all the aerodynamic force, moment and stability coefficients.

- **The engine model** returns the total thrust output from the engine in pounds of thrust and includes the afterburner effect. The thrust is a function of the throttle setting (0-100%) of the engine.

- **The upper and lower bounds** for the aircraft controls, which are given below for this aircraft model.

$$-25^{\circ} \leq \delta_{el} \leq +25^{\circ}$$

$$-21.5^{\circ} \leq \delta_{ail} \leq +21.5^{\circ}$$

$$-30^{\circ} \leq \delta_{rud} \leq +30^{\circ}$$

$$0 \leq \delta_{th} \leq 100$$

From the above bounds, the elevator cannot exceed $\pm 25°$ of deflection, the ailerons cannot exceed $\pm 21.5°$ and the rudder cannot exceed $\pm 30°$ of deflection. Also, the thrust demanded from the engine in terms of the throttle setting is between 0 and 100%.

3.1.1 Aerodynamic Model

The aerodynamic model provides the data and mathematical relations for computing the six body force and moment coefficients. These coefficients represent the three x, y and z axes body force coefficients (C_X, C_Y, C_Z), and, the three moment coefficients (C_L, C_M, C_N) corresponding to rolling, pitching and yawing respectively. These coefficients are given in Equations (21)-(26) as functions of the respective flight state and control inputs [13]. The subscript 'b' will henceforth be removed from all subsequent equations since it is understood that all flight equations are in a body-frame of reference.

$$C_X(\alpha, \delta_{el}, V_T) = C_x(\alpha, \delta_{el}) + \left[0.5\bar{c}\,\frac{\bar{q}}{V_T}\right] C_{x_q}(\alpha) \tag{21}$$

$$C_Y(\alpha, \beta, \delta_{ail}, \delta_{rud}, V_t) = C_y(\alpha, \beta, \delta_{ail}, \delta_{rud}) + \left[\frac{\bar{b}}{2V_T}\left(C_{y_r}(\alpha)\, r + C_{y_p}(\alpha)\, p\right)\right] \tag{22}$$

$$C_z(\alpha, \beta, \delta_{el}, V_T) = C_z(\alpha, \beta, \delta_{el}) + \left[0.5\,\bar{c}\,\frac{\bar{q}}{V_T}\right] C_{z_q}(\alpha) \tag{23}$$

$$C_L(\alpha, \beta, \delta_{ail}, \delta_{rud}, V_T) = C_l(\alpha, \beta) + \left[C_{l_{ail}}(\alpha, \beta)\left(\frac{\delta_{ail}}{20}\right)\right] + \left[C_{l_{rud}}(\alpha, \beta)\left(\frac{\delta_{rud}}{30}\right)\right] + \left[\frac{\bar{b}}{2V_T}\left(C_{l_r}(\alpha)\, r + C_{l_p}(\alpha)\, p\right)\right] \tag{24}$$

$$C_M(\alpha, \beta, \delta_{el}, V_T) = C_m(\alpha, \delta_{el}) + \left[0.5\,\bar{c}\,\frac{\bar{q}}{V_T}\right] C_{m_q}(\alpha) + \left[C_Z(\alpha, \beta, \delta_{el}, V_T)\,\frac{\bar{b}}{\bar{c}}\left(x_{cg_r} - x_{cg}\right)\right] \tag{25}$$

$$C_N(\alpha, \beta, \delta_{ail}, \delta_{rud}, V_T) = C_n(\alpha, \beta) + \left[C_{n_{ail}}(\alpha, \beta)\left(\frac{\delta_{ail}}{20}\right)\right] + \left[C_{n_{rud}}(\alpha, \beta)\left(\frac{\delta_{rud}}{30}\right)\right] + \left[\frac{\bar{b}}{2V_T}\left(C_{n_r}(\alpha)\, r + C_{n_p}(\alpha)\, p\right)\right] - \left[C_Y(\alpha, \beta, \delta_{ail}, \delta_{rud}, V_t)\,\frac{\bar{b}}{\bar{c}}\left(x_{cg_r} - x_{cg}\right)\right] \tag{26}$$

These coefficients are subsequently converted to their respective body forces and moments magnitudes as shown in Equations (27)-(32). The forces and moments given below are purely aerodynamic quantities. For the case of the total force experienced by the aircraft in the x-axis, the engine thrust (T) is added to the aerodynamic x-axis body force (F_X) using the thrust output from the engine model.

$$F_X = \bar{q}\, \bar{S}\, C_X(\alpha, \delta_{el}, V_T) \tag{27}$$

$$F_Y = \bar{q}\, \bar{S}\, C_Y(\alpha, \beta, \delta_{ail}, \delta_{rud}, V_t) \tag{28}$$

$$F_z = \bar{q}\bar{S}\, C_Z(\alpha, \beta, \delta_{el}, V_T) \tag{29}$$

$$L = \bar{q}\, \bar{S}\, \bar{b}\, C_L(\alpha, \beta, \delta_{ail}, \delta_{rud}, V_T) \tag{30}$$

$$M = \bar{q}\, \bar{b}\, \bar{c}\, C_M(\alpha, \beta, \delta_{el}, V_T) \tag{31}$$

$$N = \bar{q}\, \bar{S}\, \bar{b}\, C_N(\alpha, \beta, \delta_{ail}, \delta_{rud}, V_T) \tag{32}$$

3.1.2 Engine Model

The engine model provides the total thrust force generated by the engine in the F-16 aircraft model. The thrust produced is a function of the relevant flight states and control parameter as given below -

$$T = T\ (\rho, \delta_{th}, Mach) \tag{33}$$

The engine model interpolates among the thrust data contained within using the conditions given i.e. the density (which depends on altitude), throttle setting and Mach number, and returns the thrust in pounds of force.

3.2 Generic Business Jet Aircraft Model

This is a nonlinear aircraft model of a generic business jet which contains experimental data from a NASA wind tunnel study of a business jet with t-tail. The model also uses handbook methods from aircraft design references to compute the required aerodynamic data. The model consists of the following components - [13]

- **Aerodynamic Model** which contains data tables with aerodynamic coefficient data for an α range of $-10°$ to $+90°$. This data is used to determine all the aerodynamic force, moment and stability coefficients.

- **The engine model** gives the total thrust output from the engines. The thrust at any altitude is assumed to be proportional to the air density ratio raised to a power that fits the static thrust at sea level and thrust required at max Mach number and altitude.

- **The upper and lower bounds** of the aircraft controls -

$$-20^{\circ} \leq \delta_{el} \leq +20^{\circ}$$

$$-35^{\circ} \leq \delta_{ail} \leq +35^{\circ}$$

$$-35^{\circ} \leq \delta_{rud} \leq +35^{\circ}$$

$$0 \leq \delta_{th} \leq 100$$

3.2.1 Aerodynamic Model

The aerodynamic model provides, as stated earlier, aerodynamic forces in terms of the lift, drag, sideforce coefficients. It also provides aerodynamic moment coefficients of pitching, rolling and yawing. The expressions in the model are shown in Equations (34)-(39) and are written as functions of their respective state and control inputs [13].

$$C_{Drag}(\alpha) \;=\; C_{Drag_{static}}(\alpha) \tag{34}$$

$$C_Y(\alpha, \beta, \delta_{ail}, \delta_{rud}) = \left[C_{y_\beta}(\alpha, \beta)\;\beta\;\right] + \left[\;C_{y_{\delta_{ail}}}\;\delta_{ail}\right] + \left[C_{y_{\delta_{rud}}}\;\delta_{rud}\right] \tag{35}$$

$$C_{Lift}(\alpha, \delta_{el}, V_T) = C_{Lift_{static}}(\alpha) + \;\left[C_{Lift_q}(V_t)\;\;q\right] \;+\; \left[C_{Lift_{\delta_{el}}}(\alpha)\;\delta_{el}\right] \tag{36}$$

$$\begin{aligned} C_L(\alpha, \beta, \delta_{ail}, \delta_{rud}, V_T) \\ &= \left[C_{l_\beta}(\alpha, \beta)\;\beta\right] \;+\; \left[C_{l_{ail}}(\alpha)\;\delta_{ail}\right] + \left[C_{l_{rud}}(\alpha)\;\delta_{rud}\right] \\ &+ \left[\frac{\bar{b}}{2V_T}\Big(\;C_{l_r}(\alpha)\;r\;+ C_{l_p}(\alpha)\;p\Big)\right] \end{aligned} \tag{37}$$

$$\begin{aligned} C_M(\alpha, \delta_{el}, V_T) = C_{m_{static}}(\alpha) + \left[-\;C_{m_q}(V_t)\;q\right] + \left[C_{m_{\delta_{el}}}(\alpha)\;\delta_{el}\right] \\ - \left[C_{Lift}(\alpha, \delta_{el}, V_T)\;SMI\right] \end{aligned} \tag{38}$$

$$\begin{aligned} C_N(\alpha, \beta, \delta_{ail}, \delta_{rud}, V_T) \\ &= \left[C_n(\alpha, \beta)\;\beta\right] + \;\left[C_{n_{ail}}(\alpha)\;\delta_{ail}\right] + \left[C_{n_{rud}}(\alpha)\;\;\delta_{rud}\right] \\ &+ \left[\frac{\bar{b}}{2V_T}\Big(\;C_{n_r}(\alpha)\;r + C_{n_p}(\alpha)\;p\Big)\right] \end{aligned} \tag{39}$$

The lift and drag coefficients are then converted to the x and z-axis body force coefficients using the respective direction cosines for transformation (described in Chapter 2) from wind-frame to body-frame reference, as shown – [13]

$$C_X(\alpha, \delta_{el}, V_T) = \left[-C_{Drag}(\alpha)\ \cos\alpha\right]\ +\ \ [C_{Lift}(\alpha, \delta_{el}, V_T)\ \sin\alpha] \tag{40}$$

$$C_Z(\alpha, \delta_{el}, V_T) = \left[-C_{Drag}(\alpha)\ \sin\alpha\right]\ -\ \ [C_{Lift}(\alpha, \delta_{el}, V_T)\ \cos\alpha] \tag{41}$$

Subsequently, the six body force and moment magnitudes are obtained from their respective coefficients using Equations (42)-(47) in an identical manner as the F-16 model. These forces and moments are purely aerodynamic, and the engine thrust is added to the x-axis body force to obtain the total force experienced by the aircraft in the x-axis.

$$F_X = \bar{q}\ \bar{S}\ C_X(\alpha, \delta_{el}, V_T) \tag{42}$$

$$F_Y = \bar{q}\ \bar{S}\ C_Y(\alpha, \beta, \delta_{ail}, \delta_{rud}) \tag{43}$$

$$F_Z = \bar{q}\ \bar{S}\ C_Z(\alpha, \delta_{el}, V_T) \tag{44}$$

$$L = \bar{q}\ \bar{S}\ \bar{b}\ C_L(\alpha, \beta, \delta_{ail}, \delta_{rud}, V_T) \tag{45}$$

$$M = \bar{q}\ \bar{b}\ \bar{c}\ C_M(\alpha, \delta_{el}, V_T) \tag{46}$$

$$N = \bar{q}\ \bar{S}\ \bar{b}\ C_N(\alpha, \beta, \delta_{ail}, \delta_{rud}, V_T) \tag{47}$$

3.2.2 Aerodynamic Model

The engine model provides the total thrust force generated by the two engines in the business jet model. The thrust produced is a function of the relevant flight states and control parameter as given below -

$$T = (12{,}980)(\delta_{th})\left(\frac{\rho}{1.225}\right)^{0.7}(1 - \exp\left(altitude - \frac{17{,}000}{2{,}000}\right) \quad (48)$$

The thrust at any altitude is assumed to be proportional to the air density ratio raised to a power that fits the static thrust at sea level and thrust required at max Mach number and altitude.

CHAPTER 4

TREATMENT OF AERODYNAMIC DATA FOR MILITARY JET MODEL

The aerodynamic coefficient data in the reduced order model [14] had certain discrepancies where the coefficient data in the model did not coincide adequately with the respective data in the NASA full fidelity model, for example when the dependency on lateral parameters became pronounced. The following six figures plot the variation in each of the six force and moment coefficients between the reduced order data [14] and the data from the NASA report in Reference [11]. All coefficients ($C_X, C_Y, C_Z, C_L, C_M, C_N$) are graphed at four different sideslip angle values, to understand the sensitivity on the lateral variables, over the entire angle of attack range from $-10°$ to $+45°$. Subsequently, suitable methods of treatment were implemented to ensure that the model data follows the corresponding NASA data. In all subsequent figures the solid lines represent the reduced order model data and the dashed lines are data from the NASA model. Beginning with the longitudinal coefficients, the pitching moment variation is graphed in Figure 7. The reduced order model data is plotted before and after adjustment through curve fitting and it shows better agreement with the NASA model, particularly in the low to mid-range of angles of attack. Figure 8 shows the x-axis body force coefficient variation. It is seen that there is a large deviation from the original data at $\alpha = 10°$. This may be due to an error in evaluating the average of the original data. Therefore, it is corrected by re-evaluating

the average of the dashed line curves and equating it to the x-axis force coefficient for the reduced order model.

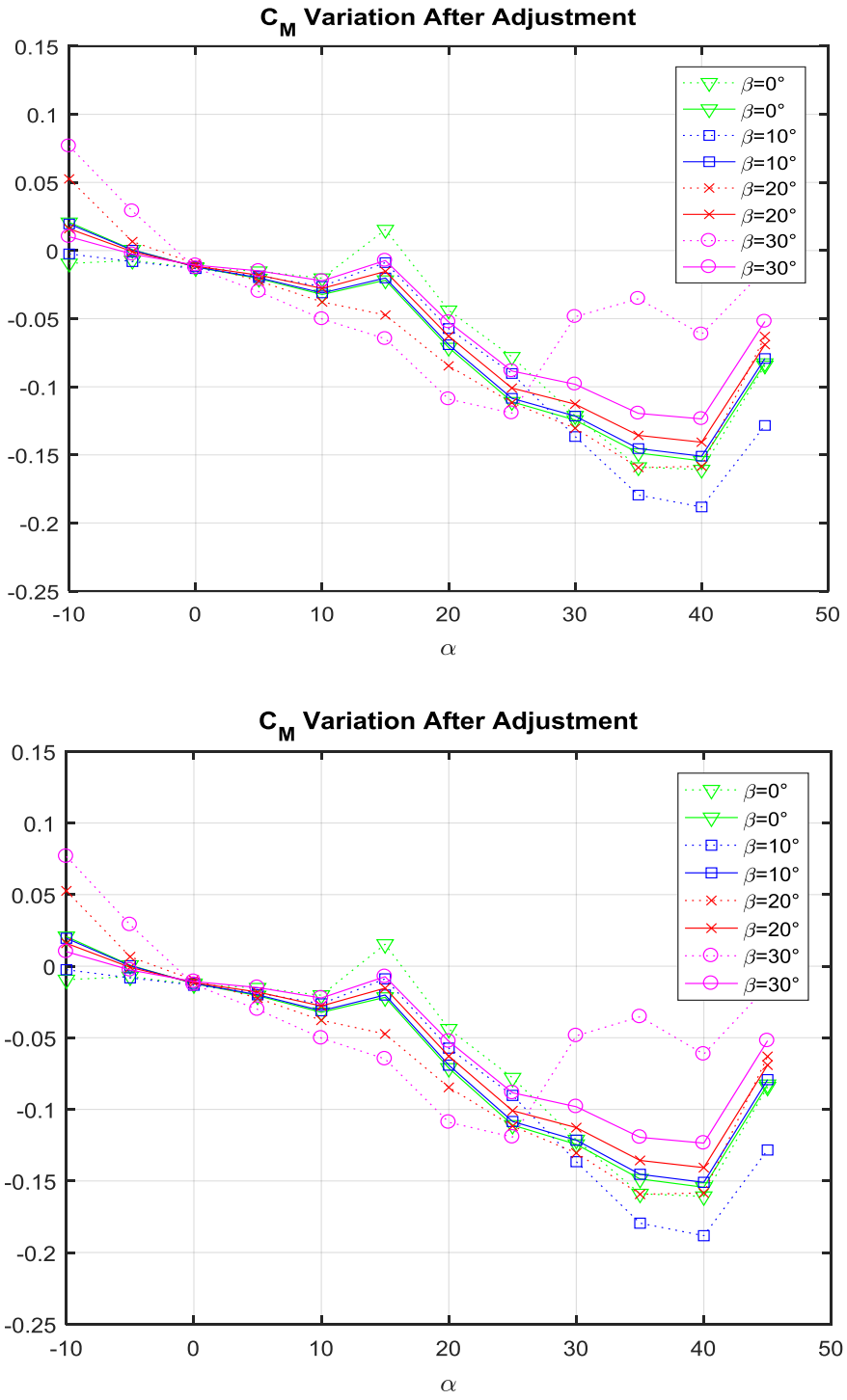

Figure 7: Pitching moment coefficient variation across the α range between model data and data from full fidelity NASA model.; (top) before adjustment of data; (bottom) after adjustment [11],[14]

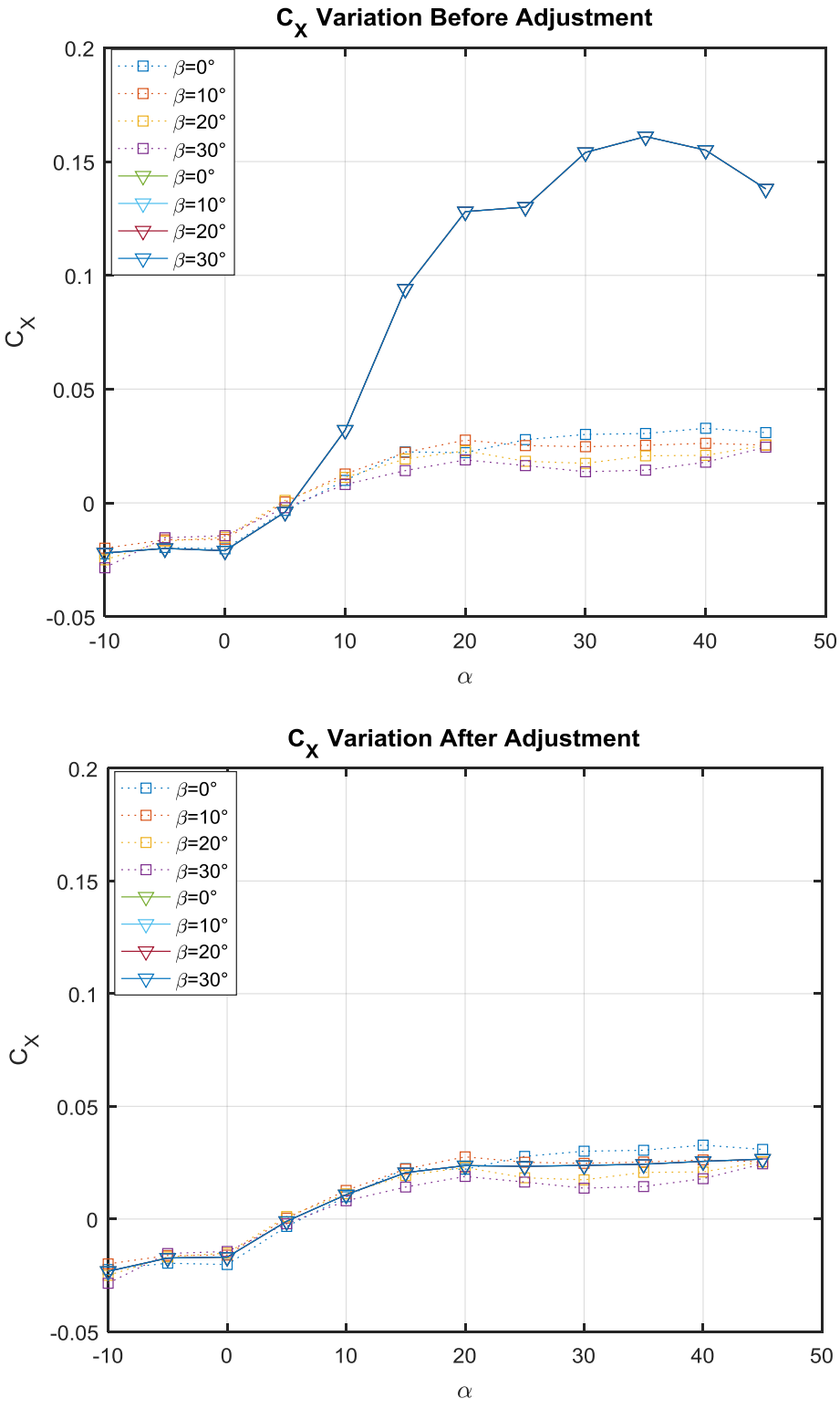

Figure 8 Axial Force Coefficient variation across the α range between model data and data from full fidelity NASA model.; (top) before adjustment of data; (bottom) after adjustment [11],[14]

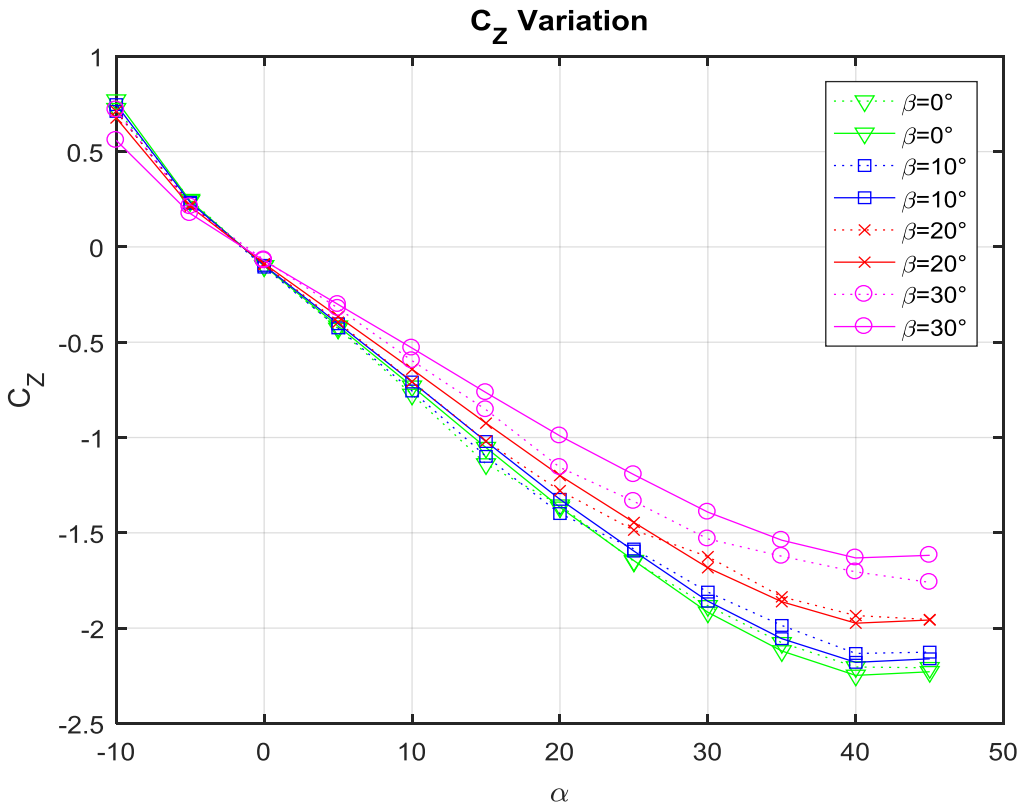

Figure 9: Vertical Axis Force Coefficient variation across the α range between model data and data from full fidelity NASA model [11],[14]

Figure 9 shows the variation in the z-axis body force coefficient and there does not appear to be any discrepancy and the data does not warrant any adjustment.

Subsequently, the lateral coefficients were studied for variation and adjusted accordingly. Figure 10 shows the variation in sideforce coefficient. Here, a linear α dependency was assumed. So, the nonlinear α dependency was brought back, since at high angles of attack the coefficient behavior is nonlinear. Figure 11 and Figure 12 graph the variation of yawing and rolling moment coefficients respectively. The data showed variation in the mid to high angle of attack range. This was adjusted for both coefficients by curve fitting and the resulting data was found to have good agreement with the corresponding original NASA data.

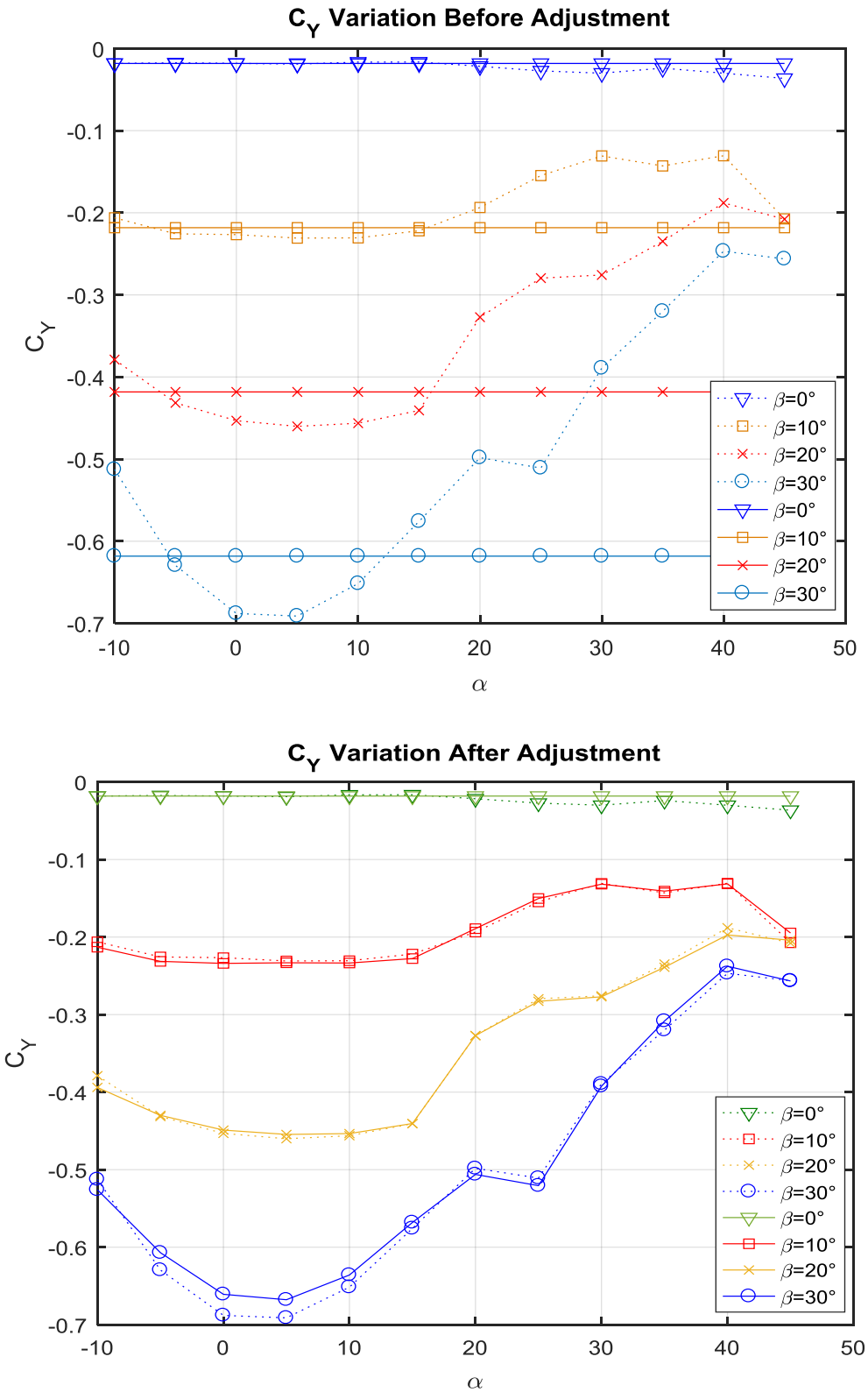

Figure 10: Side Force variation across the α range between model data and data from full fidelity NASA model.; (top) before adjustment of data; (bottom) after adjustment [11],[14]

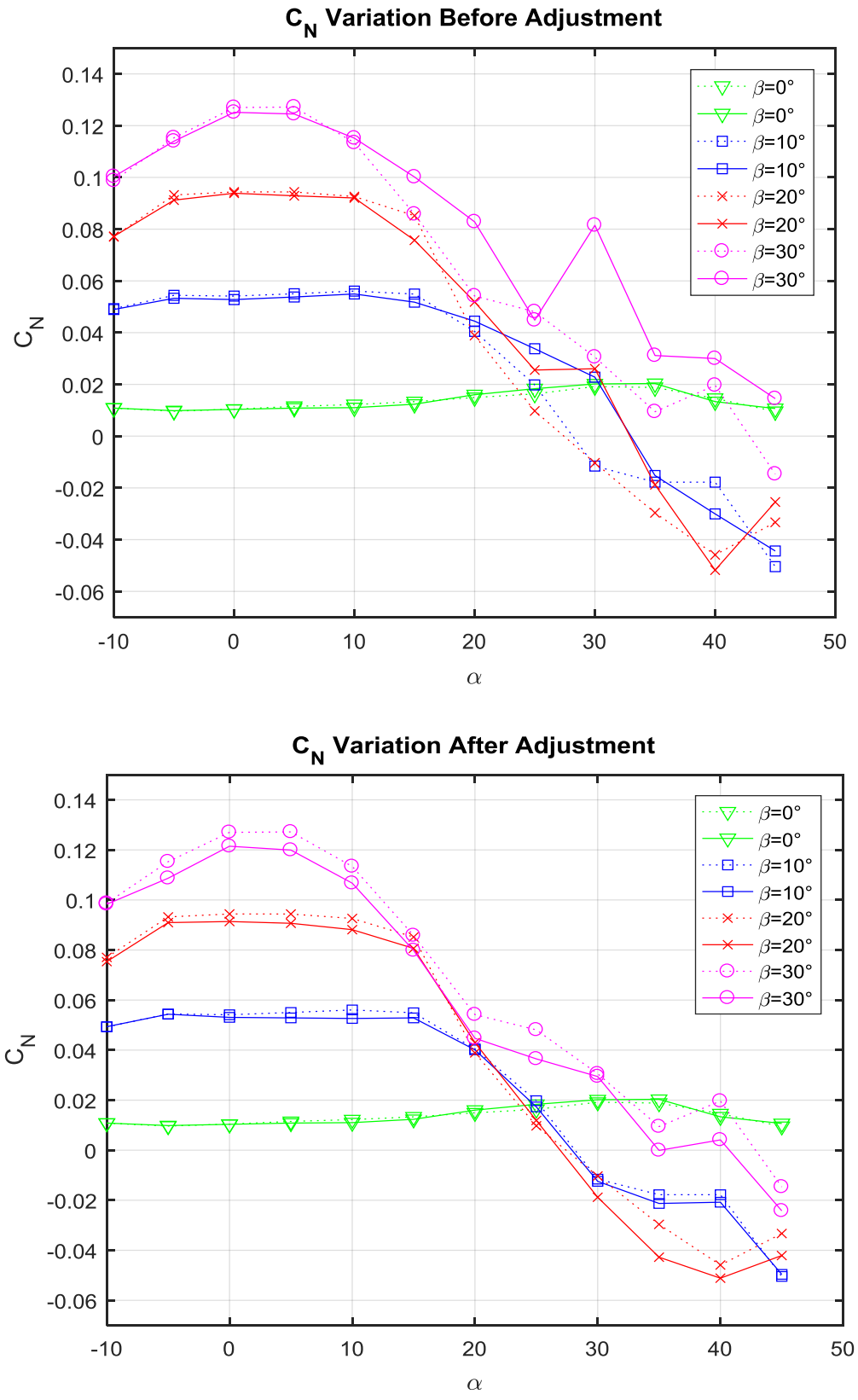

Figure 11: Yawing Moment coefficient variation across the α range between model data and data from full fidelity NASA model.; (top) before adjustment of data; (bottom) after adjustment [11],[14]

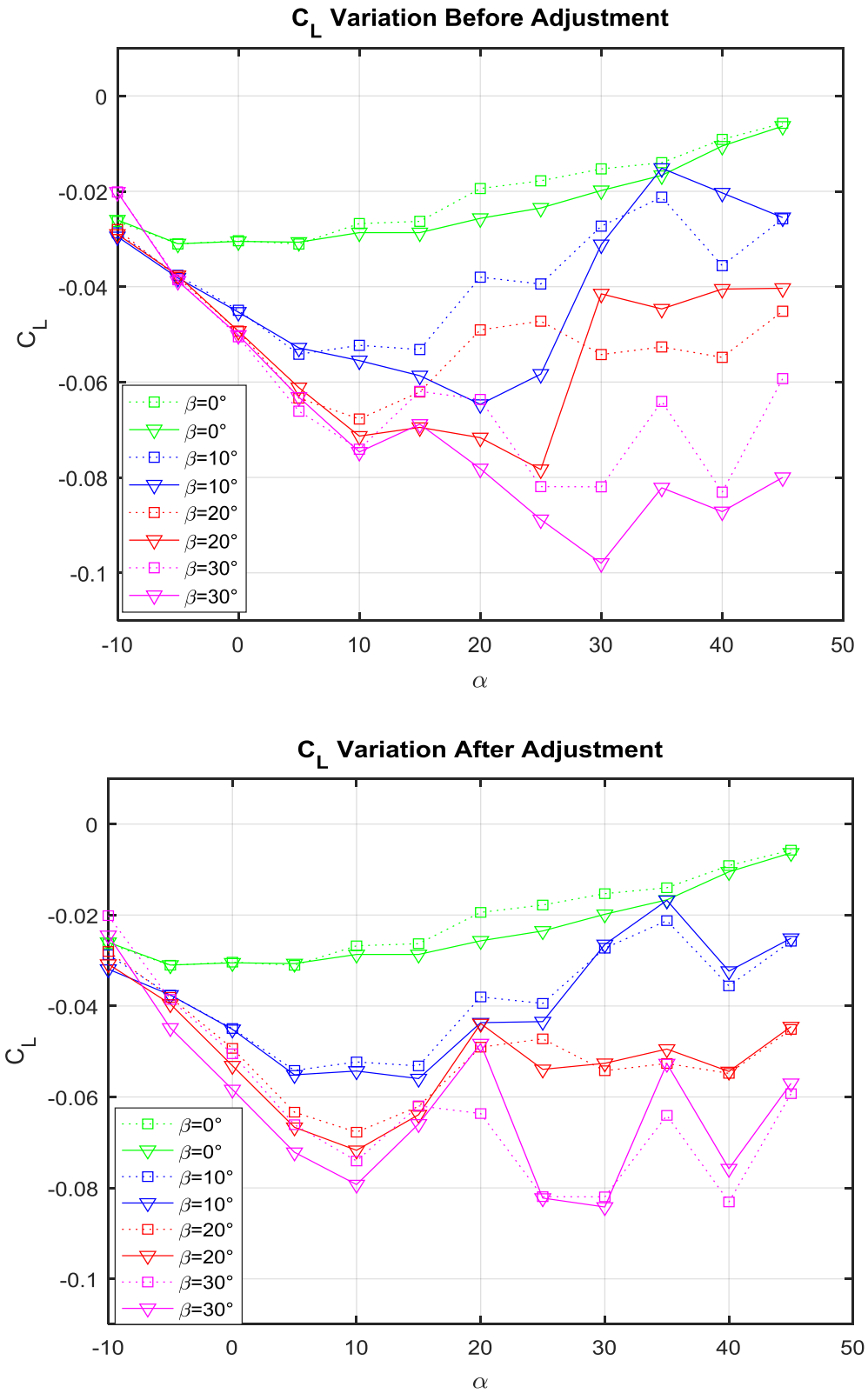

Figure 12: Rolling moment coefficient variation across the α range between model data and data from full fidelity NASA model.; (top) before adjustment of data; (bottom) after adjustment [11],[14]

This aircraft model for the provides high confidence results for the military jet, but mainly for longitudinal (and slight lateral) aircraft configurations, however, in this work, the full longitudinal and lateral extremes of aircraft trimmability is assessed. Therefore, the model is investigated and treated to ensure that the lateral aspect of flight attitudes is accounted for with the same confidence as the longitudinal aspect, as depicted in the preceding figures.

CHAPTER 5

ASYMMETRIC AERODYNAMIC ATTITUDE FLIGHT ENVELOPE

5.1 Aircraft Trimmed Flight

Since this work involves (asymmetric) trimmed flight, it is important to fully understand the nature of trim and the various variables and parameters involved. Reference [8] by Marco, Duke and Berndt provides a comprehensive overview of trim. A trim point is a flight condition where all the translational and rotational accelerations are zero. At trim, an aircraft is in a steady state or equilibrium with respect to the forces and moments acting on it. It is also easier to examine the dynamics of the aircraft in this state as the (nonlinear) equations of flight can be linearized around trim states. The stability of an aircraft can also be assessed by applying small disturbances in any of the control parameters (pitch, roll, yaw, thrust, etc.) and examining their effect on the flight path. All aircraft fly at trim during the cruise phase, which is the phase of flight relevant to this work. Trim points are also used to design and compare different models of aircraft or control systems. Trimmed flight is possible in various configurations like steady-state climb/descent, steady-state turning, horizontal wings-level flight and general straight-path flight [8],[10],[13].

The two most relevant types of steady state flight conditions are given below along with their respective properties.

5.1.1 Wings-level steady state flight

This regime requires constant speed, and wings level with the horizon. The altitude can be constant, or the aircraft can be climbing at a steady rate. Hence by definition, the roll, bank, yaw, sideslip angles as well as all the time-rates of body velocities are zero. This is the most restrictive of the steady-state regimes and requires very careful setting of the throttle, elevation, bank and flight path angles [8].

This is the flight condition shown in the traditional **speed-altitude envelope** described previously in Figure 1.

5.1.2 General Straight Flight

In this regime, roll angle, angle of attack and sideslip angle are present and considered i.e. the aircraft can be trimmed while flying (in a straight path) either at constant altitude or steady-rate climbing, with an asymmetric attitude. This can be achieved by appropriately setting the elevation, yaw, roll and thrust (using control surfaces and throttle setting). Hence, the trim controlling parameters are throttle setting, elevator deflection, aileron deflection, rudder deflection [8].

This is the trim configuration relevant to this work. The aircraft in this case is flying in a straight path at fixed altitude but with an asymmetric attitude. Figure 13 and Figure 14 show this type of rectilinear asymmetric attitude flight, where the resultant velocity vector of the aircraft is not aligned with its longitudinal body axis, but, is deviated laterally from it by the magnitude of the sideslip angle (β) [14] .

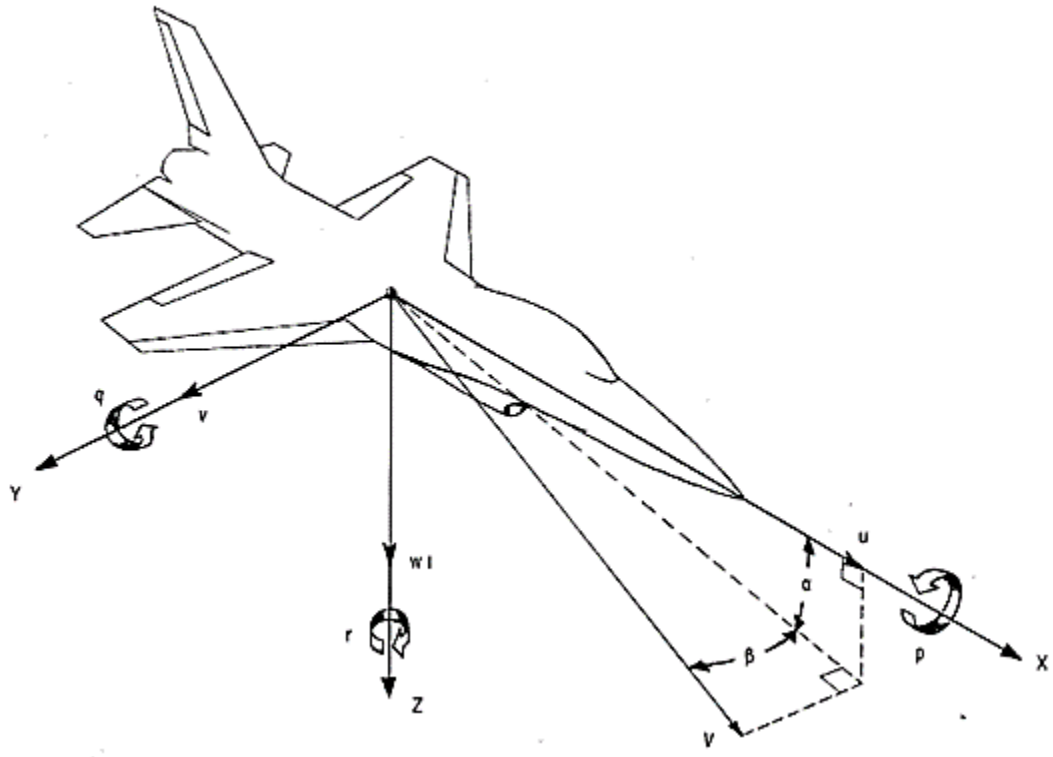

Figure 13: Depiction of asymmetric flight using body frame of reference [14]

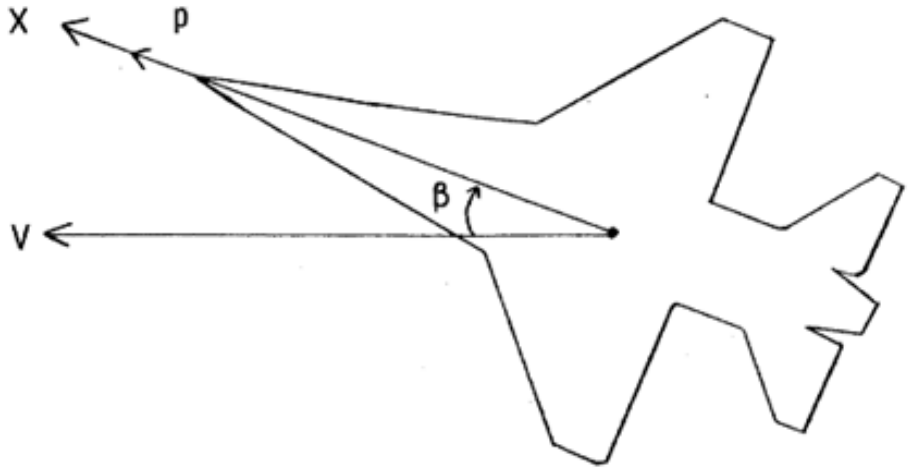

Figure 14: Top view of aircraft flying rectilinearly while sideslipping [14]

As mentioned, performance extremes are assessed for flight at this attitude by developing the asymmetric attitude flight envelope for both the military and business jet models, using a methodology that incorporates the aerodynamic models, the propulsive models and the dynamics.

5.2 Methodology of Envelope development

5.2.1 Numerical Solution Method

The equations of motion cannot be solved analytically due to the disparity between the unknowns and the equations available and hence, a numerical solution method using nonlinear optimization is employed. This method solves the equations of motion (using data from the aircraft models) and determines the trim requirements across the α-β envelope. All such points, beyond which trimmed flight is impossible under the capabilities of the aircraft form the boundary of the asymmetric attitude flight envelope. Therefore, the envelope will map the asymmetric trimmability extent for of the aircraft.

Trimmed flight mathematically corresponds to a condition of flight where the state derivatives have a zero value. These derivatives are the quantities on the LHS of the equations of motion, which are reiterated in Equations (49)-(60). These equations also contain the assumption of inertial symmetry about the x-z plane i.e. $I_{xy} = I_{yz} = 0$. This assumption was excluded from the previous equations to present the most general form of the equations of motion [1],[2].

$$\dot{u} = rv - qw - g\sin\theta + (1/m)(F_x + T) \tag{49}$$

$$\dot{v} = -ru + pw - g\sin\phi\cos\theta + (1/m)F_y \tag{50}$$

$$\dot{w} = qu - pv - g\cos\phi\cos\theta + (1/m)F_z \tag{51}$$

$$\begin{aligned} \dot{p} = [I_{zz}\{(I_{yy} - I_{zz})qr + I_{xz}\,pq + L\} + I_{xz}\{(I_{xx} - I_{yy})pq \\ - I_{xz}\,qr + N\}] / ((I_{xx}\,I_{zz} - I_{xz}^2)) \end{aligned} \tag{52}$$

$$\dot{q} = [(I_{zz} - I_{xx})pr + I_{xz}(r^2 - p^2) + M]/I_{yy} \tag{53}$$

$$\begin{aligned} \dot{r} = [I_{xz}\{(I_{yy} - I_{zz})qr + I_{xz}\,pq + L\} + I_{xx}\{(I_{xx} - I_{yy})pq \\ - I_{xz}\,qr + N\}] / ((I_{xx}\,I_{zz} - I_{xz}^2)) \end{aligned} \tag{54}$$

$$\dot{\phi} = p + \tan\theta\sin\phi\;q + \tan\theta\cos\phi\;r \tag{55}$$

$$\dot{\theta} = \cos\phi\,q - \sin\phi\,r \tag{56}$$

$$\dot{\psi} = (\sin\phi/\cos\theta)q + (\cos\phi/\cos\theta)r \tag{57}$$

$$\begin{aligned} \dot{X} = (\cos\theta\;\cos\psi)u + (-\cos\phi\sin\psi + \sin\phi\sin\theta\cos\psi) \\ + (\sin\phi\sin\psi + \cos\phi\sin\theta\cos\psi)w \end{aligned} \tag{58}$$

$$\begin{aligned} \dot{Y} = (\cos\theta\sin\psi)u + (\cos\phi\cos\psi + \sin\phi\sin\theta\sin\psi)v \\ + (-\sin\phi\cos\psi + \cos\phi\sin\theta\sin\psi)w \end{aligned} \tag{59}$$

$$\dot{Z} = -\sin\theta\,u + \sin\phi\cos\theta\,v + \cos\phi\cos\theta\,w \tag{60}$$

As stated earlier, for trimmed flight, the state derivatives must be zero, with the exceptions of $\dot{X}$, $\dot{Y}$ and $\dot{Z}$ (Equations (58)-(60)), which are the components of the translational inertial velocities of the aircraft along the respective inertial axes. Hence, for trim calculations, the **9** remaining derivatives (Equations (49)-(57)) are considered. For trimmed flight, the aircraft has to fly such that these 9 derivatives result to zero values.

The trim state calculation and boundary curve determination is formulated as a multivariable nonlinear optimization problem with bounded constraints. The optimizer tool used here is available in Matlab and uses interior-point optimization based on a trust region type algorithm.

The main components of the nonlinear optimization process are - the optimizer, the objective function and the constraints. This process works to optimize the objective function containing the mathematical representation of trimmed flight, while subjected to the constraints provided.

First, the inputs to this process must be defined, which, are the initial flight states and controls. The states are the total aircraft velocity (V_T), any point on the asymmetric attitude envelope (α, β), the body angular rates (p, q, r), the Euler angles (ϕ, θ, ψ), and, the inertial position coordinates (X, Y, Z). The state vector is accordingly given below –

$$\boldsymbol{x_s} = [V_T \quad \alpha \quad \beta \quad p \quad q \quad r \quad \phi \quad \theta \quad \psi \quad X \quad Y \quad Z]^T \tag{61}$$

The outcome of this process is to develop an envelope in terms of α and β. Therefore the (α, β) pair only is provided as a fixed input. The other inputs of flight states and controls

are initial conditions. Since the flight condition studied in this work is asymmetric trimmed straight-path flight, the body angular rates are set to zero ($p = q = r = 0$). Also, the yaw angle is set as zero degrees since the aircraft is not turning ($\psi = 0°$). The linear body velocities (u, v, w) present in the equations of motion are obtained from the total velocity magnitude, via the following trigonometric relations –

$$u = V_T \cos\alpha \cos\beta \tag{62}$$

$$v = V_T \sin\beta \tag{63}$$

$$w = V_T \sin\alpha \cos\beta \tag{64}$$

The flight control inputs are subsequently provided (as an initial input to begin optimization iterations). These controls are the flight control surface deflections (elevator, aileron and rudder) in degrees and the engine throttle setting (in percentage of total thrust), as shown–

$$\boldsymbol{u_s} = [\delta_{el} \quad \delta_{ail} \quad \delta_{rud} \quad \delta_{th}]^T \tag{65}$$

The states and controls are input to the optimizer, which initially computes the 9 aircraft state derivatives using the equations of motion and the aerodynamic and propulsion data from the selected aircraft model. These 9 derivatives are subsequently relayed as arguments to the objective function in the form of a vector, which is shown below –

$$\boldsymbol{f_d}(\boldsymbol{x_s}, \boldsymbol{u_s}) = \begin{bmatrix} \dot{u} & \dot{v} & \dot{w} & \dot{p} & \dot{q} & \dot{r} & \dot{\phi} & \dot{\theta} & \dot{\psi} \end{bmatrix}^T \tag{66}$$

The objective function receives these derivatives to check whether they correspond to a trimmed flight condition. This is done by evaluating the following mathematical expression -

$$J_d = \boldsymbol{f_d^T}(\boldsymbol{x_s}, \boldsymbol{u_s})\, R\, \boldsymbol{f_d}(\boldsymbol{x_s}, \boldsymbol{u_s}) \tag{67}$$

where, $R = diag[w_1\ w_2\ \ w_3\ w_4\ w_5\ w_6\ w_7\ w_8\ w_9]$

Here, J_d is the trim objective or cost, and, R is a diagonal matrix containing scalar weights assigned to each of the 9 derivatives in order to accelerate the optimization convergence.

If the result of calculation in Equation (67) is zero, it implies that that all 9 derivatives evaluated have a zero value, which, corresponds to a trimmed flight state, as mentioned previously. In this way, the objective function checks the derivatives for trim viability. If the trim cost is non-zero, it in turn implies that the derivatives do not satisfy trimmed flight condition.

If the trim cost (J_d) is indeed non-zero, the optimizer evaluates its proximity to a zero value, and subsequently, it appropriately alters the flight controls and attempts to converge the resulting flight state derivatives to zero.

This process is recursively repeated until the derivatives obtained are trim derivatives. The corresponding set of control variable settings used to obtain the trim derivatives are designated as the trim control settings for the given flight state inputs. These trim controls settings are recorded for each point on the asymmetric attitude envelope.

The optimizer is subject to certain constraints, as stated earlier, that limit the extent to which it can alter the flight control settings. These constraints are unique to each aircraft model, and, are given in Table 1 for the two aircraft models used in this work. These constraints correspond to the flight control parameters, the rate of climb (altitude) constraint, the maximum dynamic pressure limit and the stall limit.

The flight control parameters correspond to the constraints of the maximum deflection range of the control surfaces and the maximum throttle setting of the engine, which were mentioned earlier for both aircraft models.

The rate of climb constraint is used to ensure that the aircraft maintains a constant altitude since the α-β envelope is developed for flight at a fixed altitude. This constraint is represented by a mathematical equation that relates the flight path angle (γ) and the pitch angle (θ), along with the angle of attack (α), sideslip angle (β) and roll angle (ϕ). The flight path angle is required to be zero degrees for the aircraft to maintain constant altitude flight. Here, this constraint is used to calculate the pitch angle (for given α, β, ϕ) such that the flight path angle results to zero degrees. The pitch angle can then be used for further trim calculations as required [1].

The maximum dynamic pressure ($\bar{q}$) constraint is a structural constraint that defines the maximum speed that an aircraft can fly at such that the aerodynamic load experienced does not exceed the structural load capability of the airframe. This maximum dynamic pressure limit is unique to every aircraft and is usually provided by the manufacturer. In the case of the military jet model, the maximum dynamic pressure value was obtained from Reference [1] which utilizes a different aircraft model but is based on the same aircraft (F-16). The business jet dynamic pressure limit was obtained through review of the maximum operating speed of an identically dimensioned and configured business jet with a T-tail.

The stall constraint, which dictates the minimum speed that an aircraft can fly without encountering the aerodynamic stall phenomenon, is also incorporated into the optimization algorithm. This minimum speed, for both aircraft models varies with the sideslip angle being investigated.

Table 1: Trim Optimization Constraints for Both Aircraft Models

Military jet model	Business jet model
Flight Control Constraints	
$-25^{\circ} \leq \delta_{el} \leq +25^{\circ}$	$-20^{\circ} \leq \delta_{el} \leq +20^{\circ}$
$-21.5^{\circ} \leq \delta_{ail} \leq +21.5^{\circ}$	$-35^{\circ} \leq \delta_{ail} \leq +35^{\circ}$
$-30^{\circ} \leq \delta_{rud} \leq +30^{\circ}$	$-35^{\circ} \leq \delta_{rud} \leq +35^{\circ}$
$0 \leq \delta_{th} \leq 100$	$0 \leq \delta_{th} \leq 100$
Rate of Climb Constraint	
$0 = -\sin\gamma + (\cos\alpha \cos\beta)\sin\theta + (\sin\phi \sin\beta + \cos\phi \sin\alpha \cos\beta)\cos\theta$	
Dynamic Pressure Constraint (For V_{Max})	
$\bar{q} \leq 2750\ \mathrm{lb/ft^2}$	$\bar{q} \leq 25630\ \mathrm{kg/ms^2}$
Stall Constraint (For V_{Min})	
Stall condition varies with β	Stall condition varies with β

In summary, there are 7 constraints, 12 flight states and 4 control variables that are utilized by the envelope development algorithm (in conjunction with the aircraft aerodynamic and engine models, and the equation of motion,) to compute the trim control settings at a given point in the envelope. Subsequently, all such points where a trim solution is possible are

said to exist inside the asymmetric attitude envelope, and, all points where trim solution is impossible, exist outside the envelope since the aircraft cannot be trimmed at those attitudes. It follows then, that the boundary of the envelope constitutes all such couples of (α, β) beyond which the aircraft is not trimmable [1]. Hence, the full extent to which an aircraft can be trimmed while having asymmetric attitudes is known.

Through this methodology, the asymmetric attitude envelope boundary can be developed for any aircraft model. Additionally, the asymmetric attitude performance data computed at every point in the envelope is highly useful and is recorded for further analyses and review. Figure 15 illustrates this methodology using a schematic flowchart.

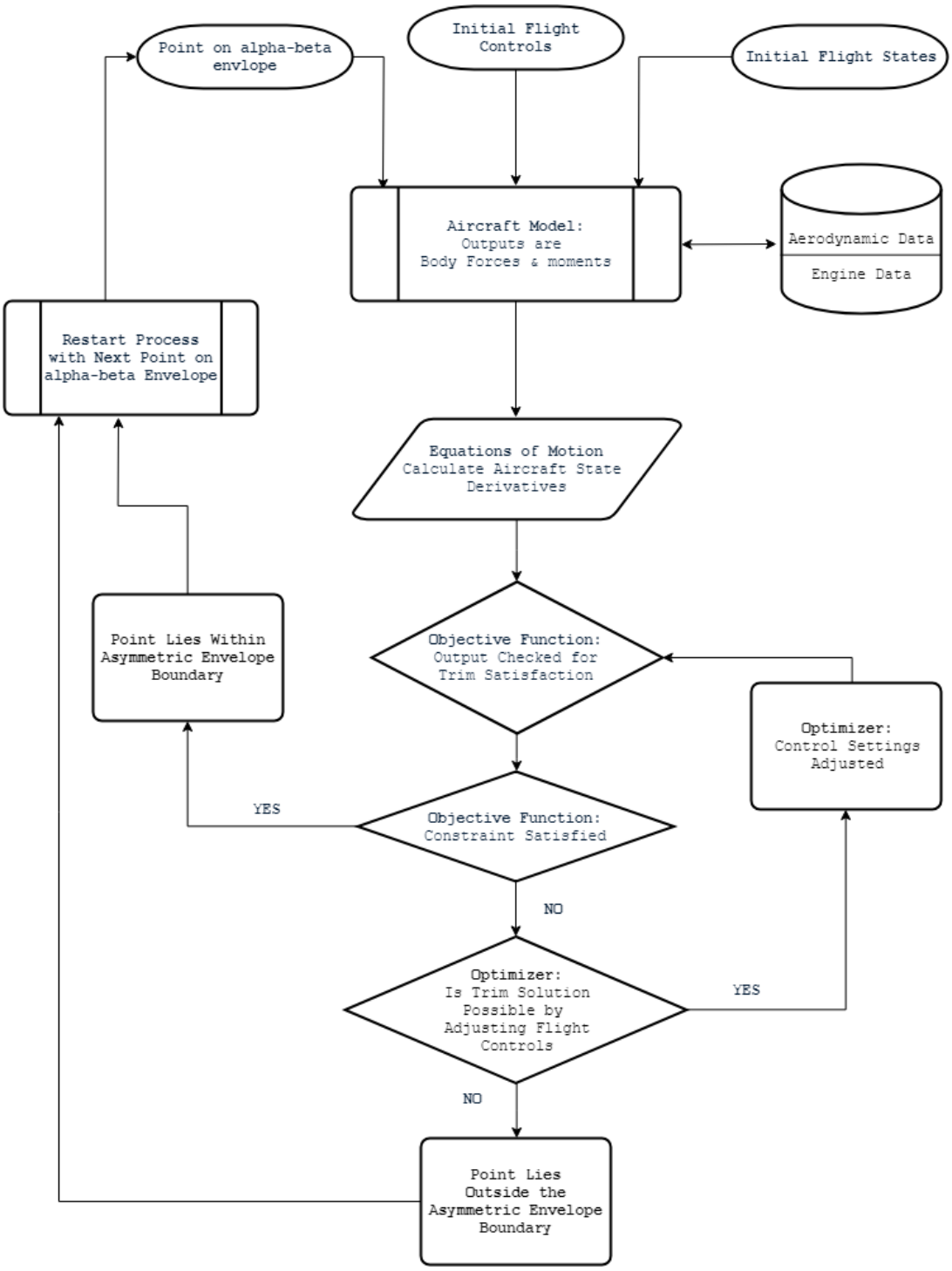

Figure 15: Flowchart showing Envelope Development Process

For validation of the envelope development algorithm, it is necessary to compare the output in terms of the trim control requirements to those from the source references (for the same inputs). Hence, known trim inputs and outputs from References [13] and [14] were tested to ensure the algorithm produced the same results as the respective references. Additionally, any output of control settings produced by the algorithm may be substituted back into the equations of motion to ensure that they result in zero values for all 9 aircraft derivatives concerned.

The constrained optimizer used can also be customized to suit accuracy requirements, for example, the objective function tolerance can be altered along with number of iterations, number of function evaluations, type of optimization algorithm used, etc., giving the user control (to an extent) of the accuracy of the results produced. For this work, all tolerances were set to 1.0×10^{-12} and maximum function evaluation and iterations were each set to 5000.

CHAPTER 6

RESULTS AND DISCUSSION

6.1 Results for Military Jet Model

The following Figure 16 shows the asymmetric attitude flight envelope developed for the F-16 fighter aircraft model at sea level altitude. This envelope shows angle of attack vs. sideslip angle (α-β) and describes the asymmetric trimmablility extent of this aircraft for the entire range of data available. From Figure 16, it is observed that the maximum sideslip boundary is about $\pm 20°$ and occurs at an angle of attack of $19°$. From this point, the envelope boundary gradually converges and approaches the zero sideslip line as the angle of attack rises. It should be noted above $45°$ angle of attack, the envelope boundary is developed by extrapolation of available aerodynamic coefficient data since the model only has data for $-10°$ to $+45°$ range of α. Above $45°$, ultimately, the envelope boundary closes at $46.3°$ angle of attack. Since it is known that the aircraft is trimmable at extended angles of attack and zero sideslip angle, and due to the limited availability of model data, the aerodynamics in the angle range greater than $45°$ are extrapolated. The envelope information in this extrapolated region can provide useful flyability information, however, the reliability of such information should be considered further to account for the highly nonlinear and unstable aerodynamics due to (numerical) stall and post stall effects encountered at this high α range. Hence, the extrapolated upper boundary is

plotted using dashed lines in Figure 16 and the results in this region are not assumed to be as accurate as those in the region below for which coefficient data is given.

Indicated on the envelope boundary, between the marking points, are the zones where the respective control surfaces were the limiting factors that caused the envelope boundary to be reached. For instance, between angles of attack range $-10°$ to $+18.8°$, the maximum rudder deflection limit was the limiting factor i.e. in this zone the aircraft reached its trimmability limit because the rudder could no longer compensate for the sideslip and provide sufficient lateral force and moment to trim the aircraft.

Immediately above the rudder limit zone lies the aileron limit zone from $18.9°$ to $28.9°$ angle of attack. In this region of the boundary, the aileron, even at its max deflection, failed to provide enough control to trim the aircraft.

The rudder and aileron switch zones again at angle of attack of $37.8°$ until the top of the envelope where aerodynamic stall is the main limiting factor, as discussed previously.

In this manner, from the trim data generated during the envelope development, it is possible to know the trim requirements at any orientation of the aircraft within the envelope boundary.

Below the center of the envelope (i.e. the origin), starting at $\alpha = -1.3°$, the aircraft flies at an inverted orientation as shown in Figure 16. The aircraft in this region has transitioned from the upright attitude to an inverted one. This is because the trim requirements in this region are such that the aircraft can only fly trim in the upside-down position i.e. the roll angle is required to be greater than $90°$. The boundary in this region is shown as dashed lines in Figure 16.

Since the aircraft concerned is an agile and maneuverable fighter jet, flight in the inverted attitude is acceptable, as it is part of the operating mission of the aircraft. Hence, the inverted trim region falls within the operating envelope of the aircraft.

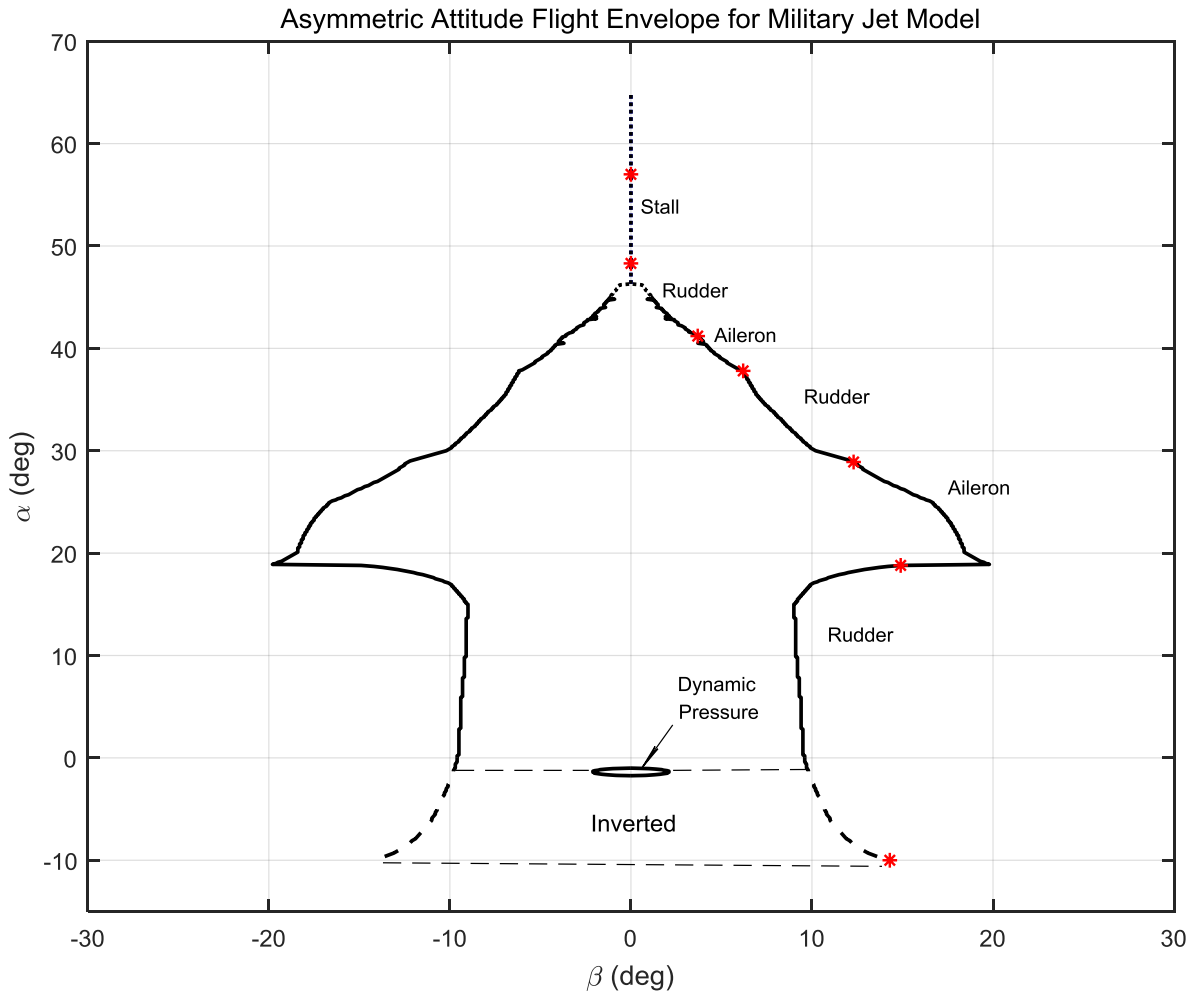

Figure 16: Asymmetric Attitude Flight Envelope for F-16 Military Jet Model

From Figure 16 just below the $\alpha = 0°$ point, lies another type of flight operating limit called the maximum dynamic pressure limit (or maximum $\bar{q}$-limit). It is represented here by a small ellipsoid region. All aircraft have a maximum dynamic pressure limit, which is $2750\frac{lb}{ft^2}$ for the F-16 aircraft model. This limit remains constant for any altitude and arises from the structural loading limitation and maximum thrust available for the aircraft.

During envelope boundary development, this limit is added as a constraint on the optimizer to ensure that the aircraft never exceeds the dynamic pressure limit. Hence, within the $\bar{q}$-limit region, trimmed flight is not possible as it would exceed the dynamic pressure limit. An enlarged image of $\bar{q}$-limit region is shown in Figure 17. The outer boundary of this bubble-shaped region corresponds to the highest-speed region of envelope where the aircraft speed reaches Mach 1.3 for the F-16 model. However, as the altitude increases, the dynamic pressure limit is expected to disappear and replaced by the maximum thrust limit of the engine. This observation can be inferred from the speed-altitude envelope in Figure 1.

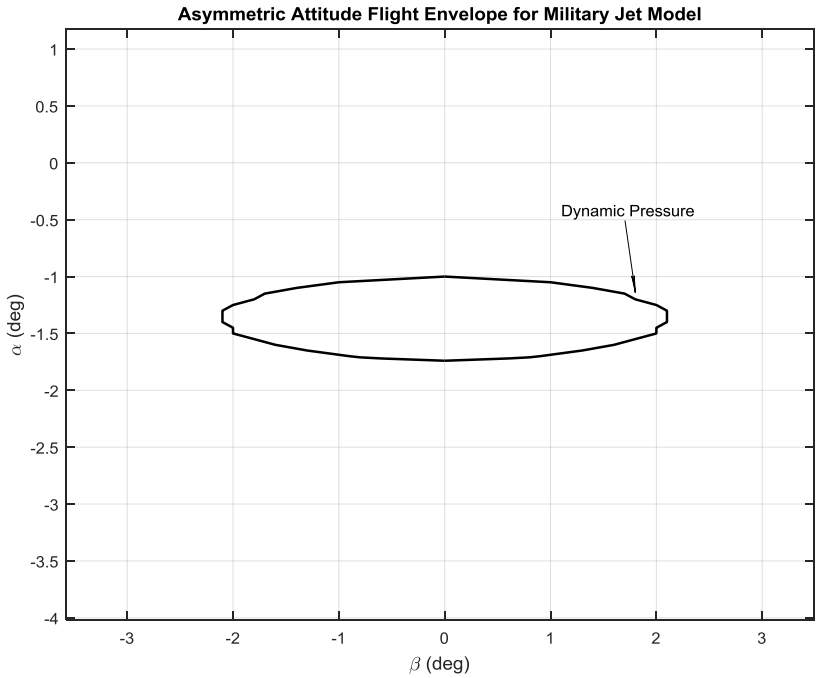

Figure 17: Enlarged section of envelope showing the maximum dynamic pressure limit region

The envelope also appears to be truncated at the $-10°$ angle of attack point. This is due to unavailability of aerodynamic data beyond this point. However, moving further down, the F-16 is still capable of trimmed inverted flight. So, to observe the trimmability beyond this point, the aerodynamics would need to be extrapolated. This is however, inadvisable

since the range of extrapolation is large (tens of degrees), unlike the top of the envelope where extrapolation is carried out from $45°$ to $46.3°$ angle of attack which is a very small extrapolation range. Further, the reference in which the data for this model is present, states strongly to avoid extrapolation of such data [14].

The behavior of various flight performance parameters is analyzed by studying their variation across the asymmetric attitude envelope. Figure 18 shows contours or isolines of aircraft velocity in ft/s and Mach number for the right hand region of the α-β envelope (from the envelope center to $\alpha = 20°$). It is clearly observed that the magnitude of speed required for asymmetric trimmed flight is highest at the $\bar{q}$-limit region and decreases consistently with increasing angle of attack. The range of speed variation with angle of attack is considerable, from supersonic to low subsonic at high α. However, the variation of speed with sideslip angle (for given angle of attack) is not as dramatic, except in the region close to the maximum dynamic pressure. Figure 19 shows contours of Mach numbers in the close vicinity of the $\bar{q}$-limit region in the asymmetric attitude envelope. The speed in this region changes significantly for very small changes in sideslip angle (or angle of attack). This sudden variation of trim speed in this region implies that the aircraft can easily switch from a supersonic regime to a subsonic one by imparting a slight increase in sideslip angle, for a given angle of attack. This insight has utility for flight control systems that can shift the aircraft from supersonic to subsonic flight (and vice versa) by introducing lateral sideslip through precise manipulation of aircraft controls. Overall, these contours show the full range of velocities for asymmetric trimmed flight of the military jet model and the pattern of variation of the trim velocities across the envelope.

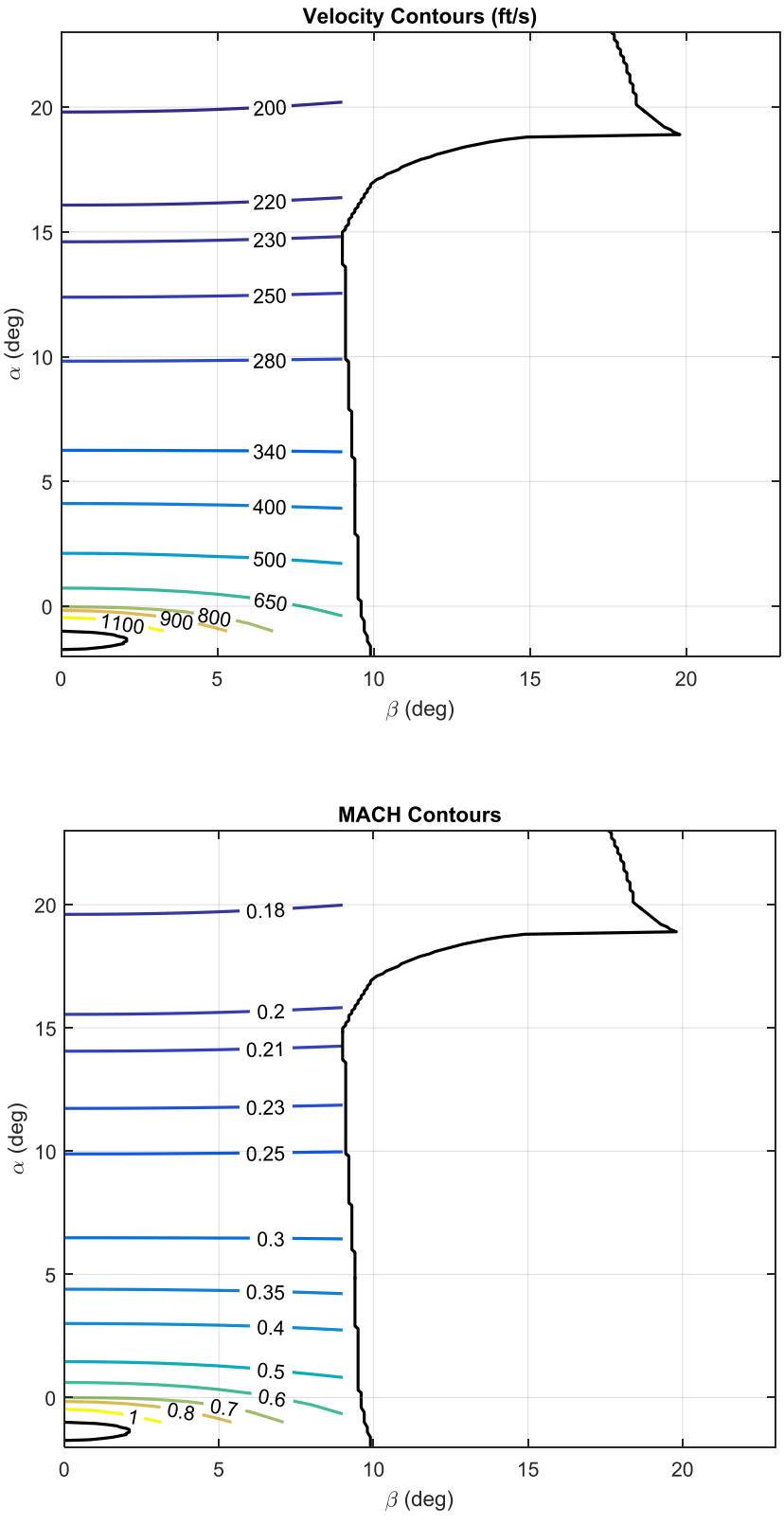

Figure 18: Trim Velocity (top) and Mach Contours (bottom) on a region of α − β Envelope

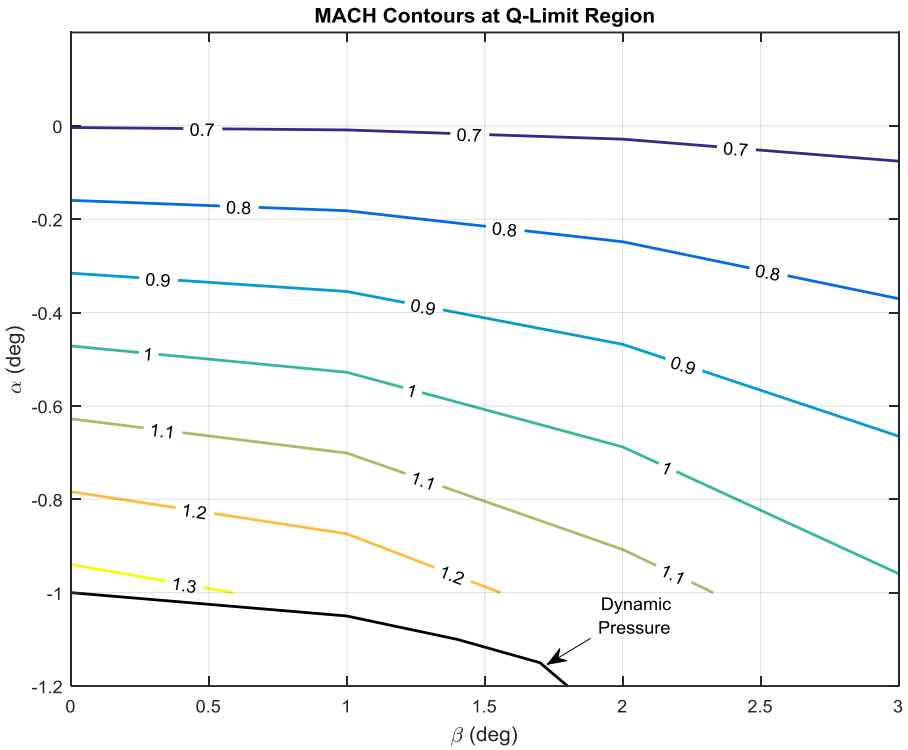

Figure 19: Contours of Mach Number Around Max Dynamic Pressure Limit

The contours of aircraft roll or bank angle (ϕ) are shown in Figure 20 for the same region of the envelope as the velocity contours. The roll angle values show variation with both angle of attack and sideslip angle. The pattern of variation shows that as the aircraft moves away from the zero-sideslip line (vertical axis line), the required roll angle increases until the boundary of the envelope. The degree of variation depends on the angle of attack and is highest near the center of the envelope. Similar to the velocity contours, the roll angle varies significantly near the maximum dynamic pressure region even for small changes in sideslip angle or angle of attack. The aircraft roll angles reach more than $70° - 80°$, with the aircraft inevitably transitioning to an inverted orientation as the α decreases further than the region shown in Figure 20. Again, this property of roll angle is a performance insight that is not visible in conventional flight envelopes and can be useful for implementation in aircraft control systems.

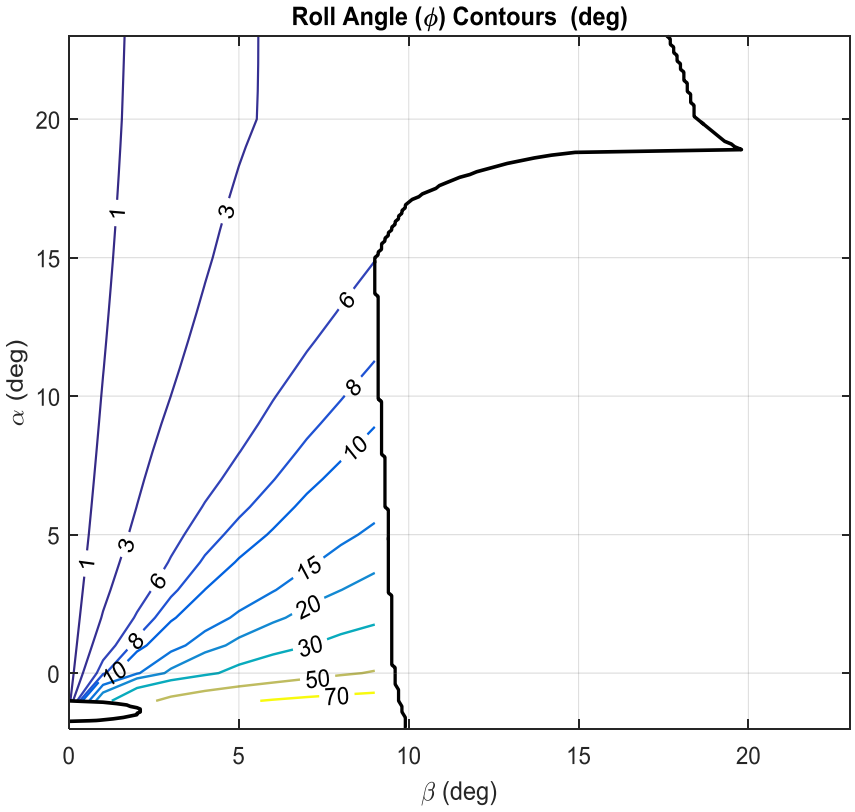

Figure 20: Trim Roll Angle Contours (deg) on a region of α − β Envelope

The trim history of the four aircraft controls ($\delta_{el}, \delta_{ail}, \delta_{rud}, \delta_{th}$) is also studied using the envelope performance data to gain a better understanding of the control requirements for asymmetric trimmed flight for the military aircraft model.

Figure 21 shows the variation of elevator deflection setting with sideslip angle at various angles of attack ranging from $-1°$ to $40°$. The elevator deflection has a range of $-25°$ to $+25°$. It is fascinating to observe that the elevator deflection is completely unaffected by change in sideslip angle and only changes with angle of attack. Also, studying the trim history of the elevator reveals that it never reaches its maximum allowed deflection, even at very high α. Such observations imply that the elevator does not play a major role in asymmetric trimmimg of the aircraft.

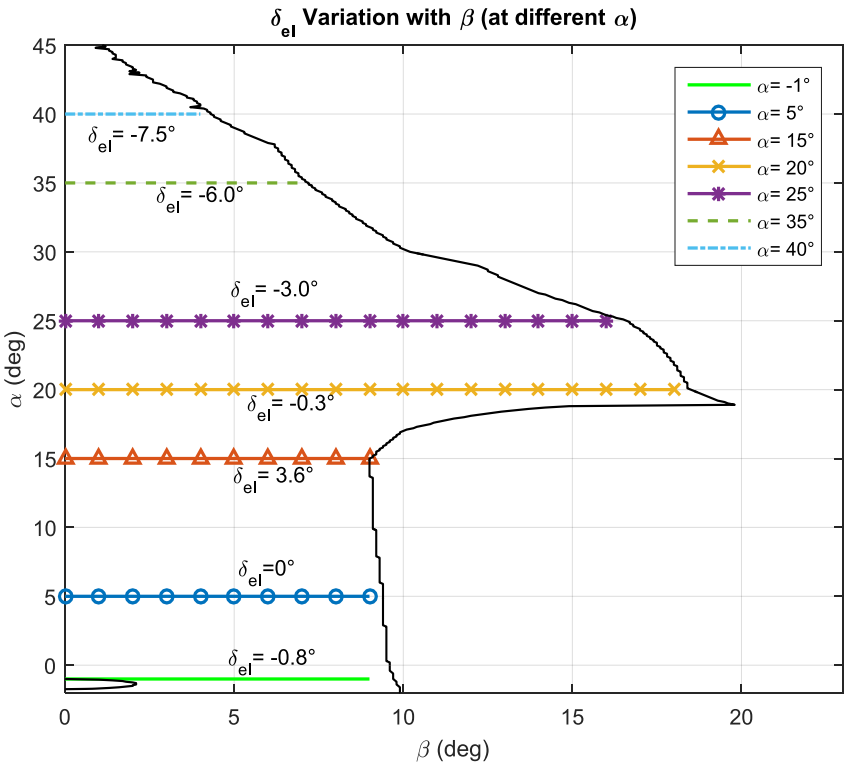

Figure 21: Variation with Sideslip angle of Trim Elevator Deflection at given α values

Figure 22 (top figure) shows the contours of trim throttle setting requirement in the region from the envelope center to $\alpha = 20°$. The throttle setting corresponds to the percentage of thrust required from the engine ($0 \leq \delta_{th} \leq 100$). The throttle requirements are highest near the dynamic pressure limit region and decrease as the angle of attack rises. However, this pattern reverses after around 4° angle of attack and the throttle setting begins to increase from low throttle to high throttle percentages. Also, at the dynamic pressure limit region, the throttle requirements change (with α and β) much more rapidly than at other regions of the envelope, similar to the behavior of the trim speed and roll angle observed previously. This property is depicted in the bottom figure of Figure 22 which shows the trim throttle settings in close vicinity of the dynamic pressure limit.

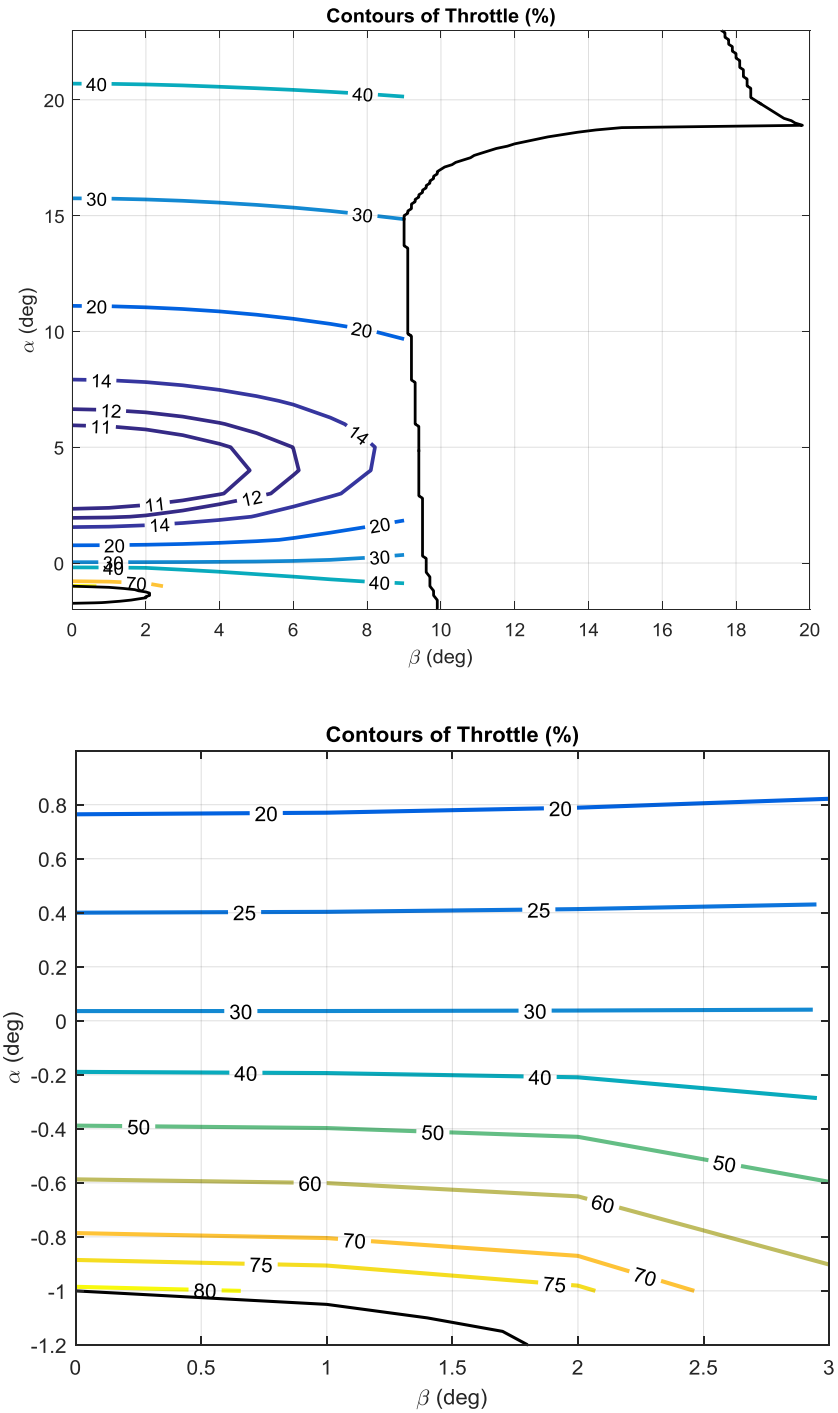

Figure 22: Trim Throttle Setting Contours on a region of Envelope (Top); Throttle Setting Contours Around the Dynamic Pressure Limit Region (Bottom)

Figure 23 also graphs the trim throttle setting but at a wider range of angles of attack from $-1°$ to $40°$, with respect to sideslip angle. Again, the δ_{th} remains almost constant with change in sideslip angle (for given α). This figure further illustrates the rapid variation of the δ_{th} near the $\bar{q}$-limit region. For instance, at $\alpha = -1°$, the throttle changes from a maximum of 80% at $\beta = 0°$ to a minimum of 40% at $\beta = 9°$. Also, very large angles of attack (above $35°$) demand significantly higher throttle settings than lower angles of attack. This speaks to the relative feasibility of sustained flight at values of α near the $\bar{q}$-limit region and α values above $35°$, versus sustained flight at low to mid range of angles of attack.

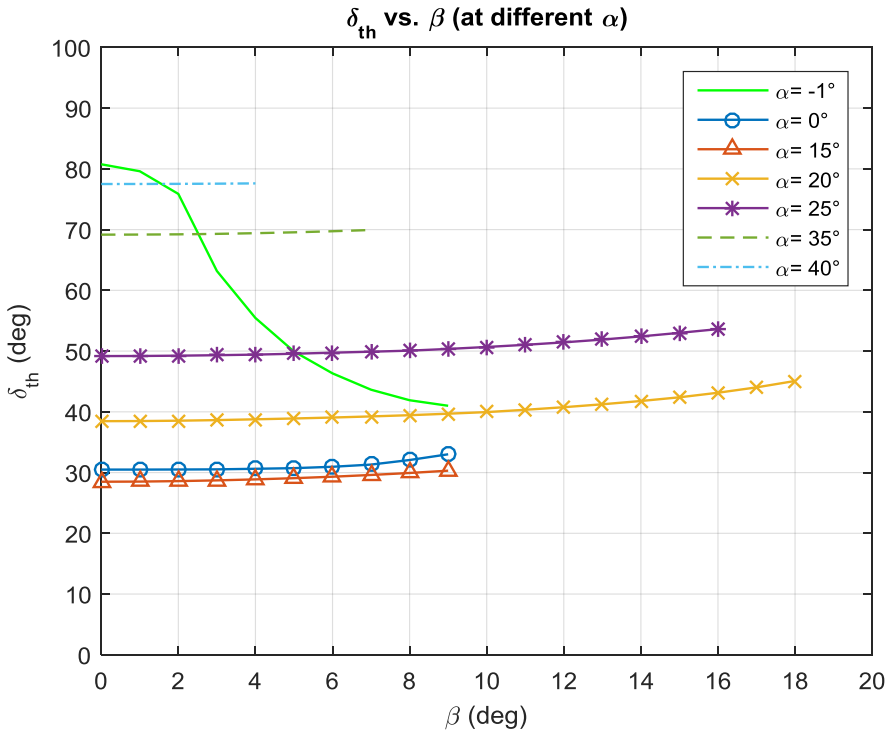

Figure 23: Variation with Sideslip angle of Trim Thrust at given α values

The rudder and aileron are control surfaces that vary in such manners that plotting contours would not provide any meaningful inferences. Hence, the variation of rudder and aileron deflection (shown in Figure 24) are graphed with respect to sideslip angle at the same angle of attack range as the previous figure. The rudder and aileron show variation with both angle of attack and sideslip angle. These control surfaces reach their maximum possible deflections for the α within their respective zones of influence within the asymmetric attitude envelope, which were discussed previously and shown in Figure 16. For a given angle of attack, moving along the deflection lines of both the rudder and aileron reveals a transition point beyond which, either the rudder or the aileron becomes more dominant and reaches its maximum deflection ($\pm 30°$ for δ_{rud} and $\pm 21.5°$ for δ_{ail}) at the boundary of the envelope. The control surface which becomes dominant is dictated by the respective zones of influence in which the given angle of attack lies. Also, in general, it can be said that in terms of deflection, the rudder and aileron are utilized relatively more than the elevator to trim the aircraft at asymmetric attitudes.

All these insights into the authority of all the control surfaces with respect to asymmetric trimmability of the aircraft are important observations in understanding the performance dynamics of the aircraft.

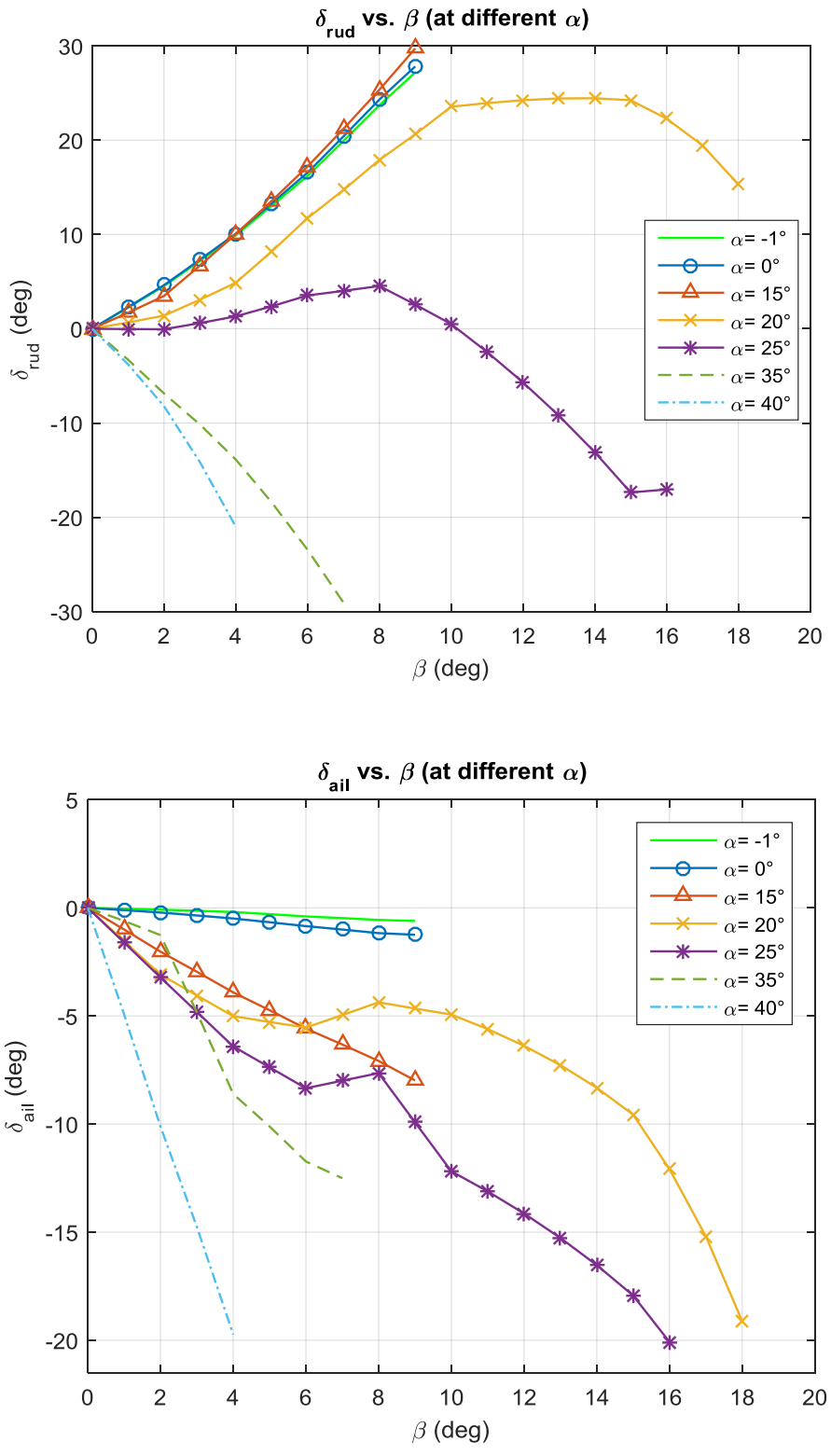

Figure 24: Variation with Sideslip angle of Trim Rudder (top) and Aileron Deflection (bottom) at given α values

6.2 Results for the Business Jet Model

Figure 25 shows the asymmetric attitude flight envelope developed for the business jet aircraft model. This envelope shows the trimmability extent of this aircraft model at asymmetric attitudes at sea level altitude. The envelope boundary encompasses the full asymmetric operability of the business jet model. The envelope extends from an α range of $1.4°$ to $26.2°$ with a maximum sideslip angle value of just over $\pm 29°$.

The maximum dynamic pressure and engine throttle limits dominate at the low range of angles of attack of the envelope boundary, whereas, in the moderate to high range of angles of attack, the aileron deflection limit is encountered, which alternates back to the thrust limit before ultimately the stall boundary occurs and the envelope concludes.

The maximum dynamic pressure limit is present from an α range of $-4°$ to $+4°$, and shifts to the maximum thrust available which spans laterally across the envelope until an β of $29.1°$ and α of $2.3°$. From this point, the maximum aileron deflection is the limiting factor up to an α of $18.8°$, and then the limiting parameter again shifts to the maximum thrust capability until eventually the envelope converges, reaching (numerical) stall at the very top of the boundary at $26.2°$ angle of attack. Beyond this point, no trim solution is possible. So, the limiting factors that define the boundary of the asymmetric attitude envelope for the business jet model are different than those for the military jet.

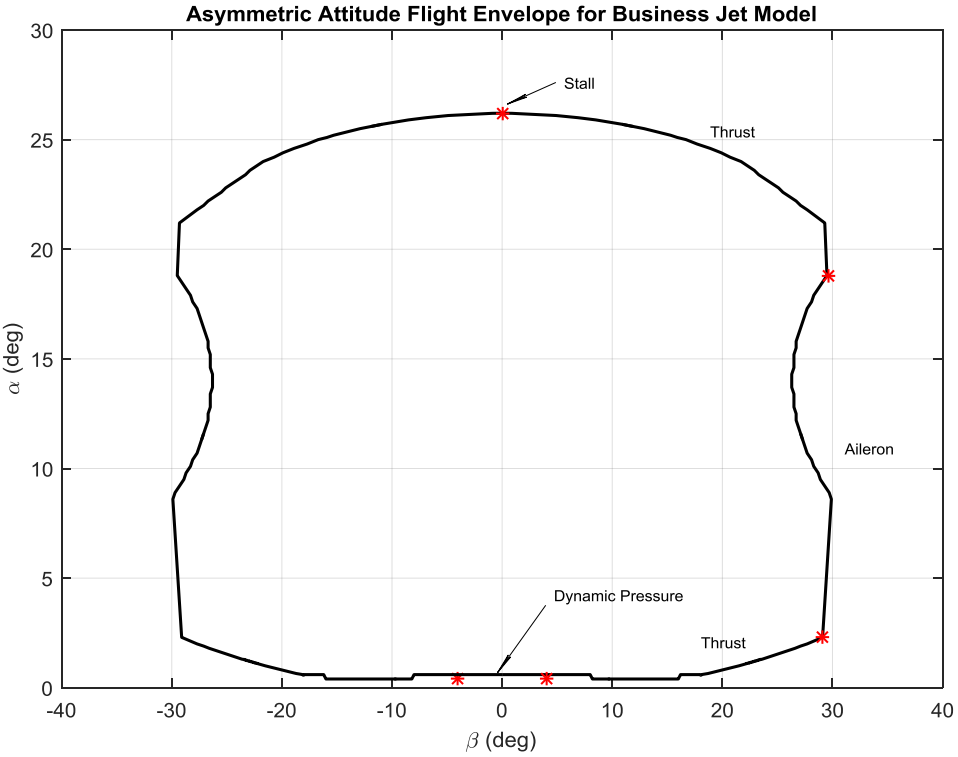

Figure 25: Asymmetric Attitude Flight Envelope for Business Jet Model

The flight performance parameters like trim velocity and roll angle are analyzed by studying their contours across the asymmetric attitude envelope. Figure 26 shows contours of velocity on a region of the α-β envelope from the envelope base to $\alpha = 10°$. It is observed that the magnitude of speed for asymmetric trimmed flight is highest at the $\bar{q}$-limit region and decreases consistently with increasing angle of attack, reaching very low subsonic speeds towards the ceiling of the envelope where the aircraft stalls. The range of speed variation with is not as wide ranging as the supersonic jet, since the maximum operating speed of this aircraft model is around Mach 0.7. The variation of speed with sideslip angle for any given angle of attack is again significant in the region close to the maximum dynamic pressure and not as significant at higher regions of the envelope.

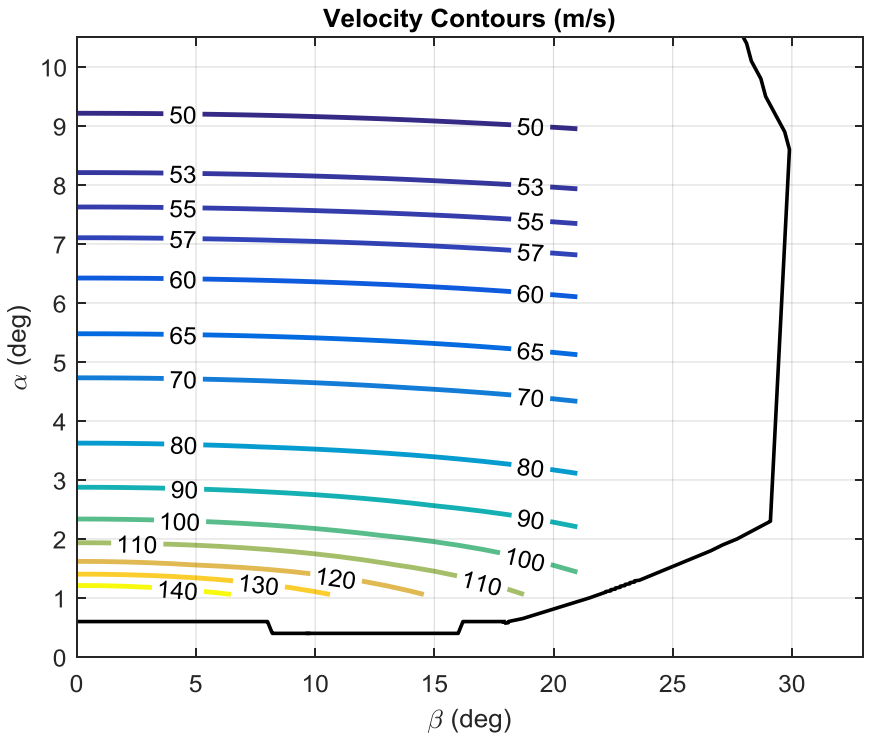

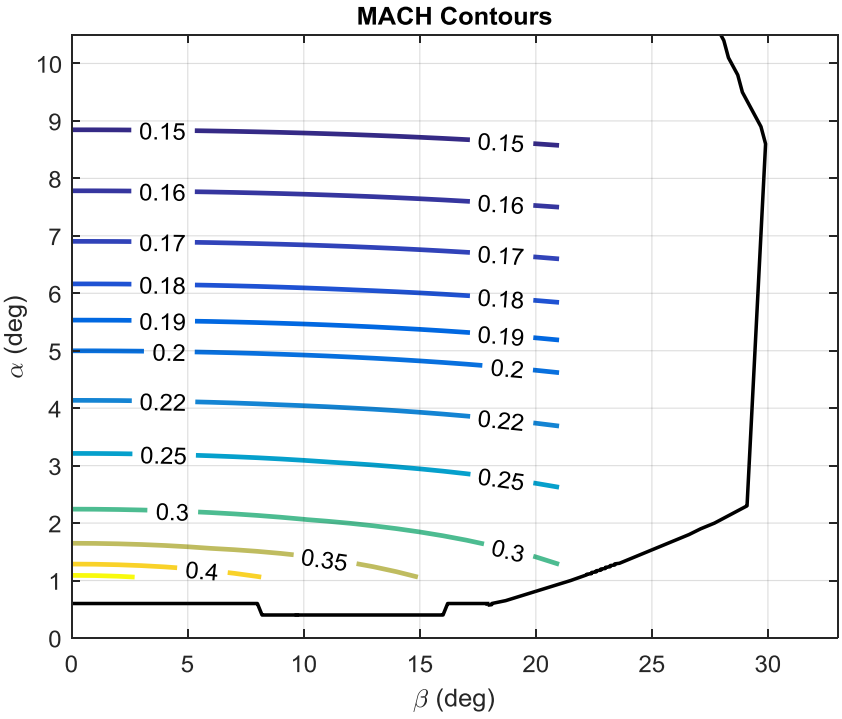

Figure 26: Trim Velocity (top) and Mach Contours (bottom) on a section of $\alpha - \beta$ Envelope

The contours of aircraft roll angle (ϕ) are shown in Figure 27 for the envelope of the business jet model. Similar to the military jet model, the roll angles show variation with both angle of attack and sideslip angle such that, as the aircraft moves away from the center of the envelope base, the required roll angle increases laterally until the boundary of the envelope. The degree of variation depends on angle of attack and is highest near the center of the envelope. The roll angle varies significantly near the highest-speed region, reaching values of 50° to 60°, which is a substantial amount of bank for a civilian business jet model.

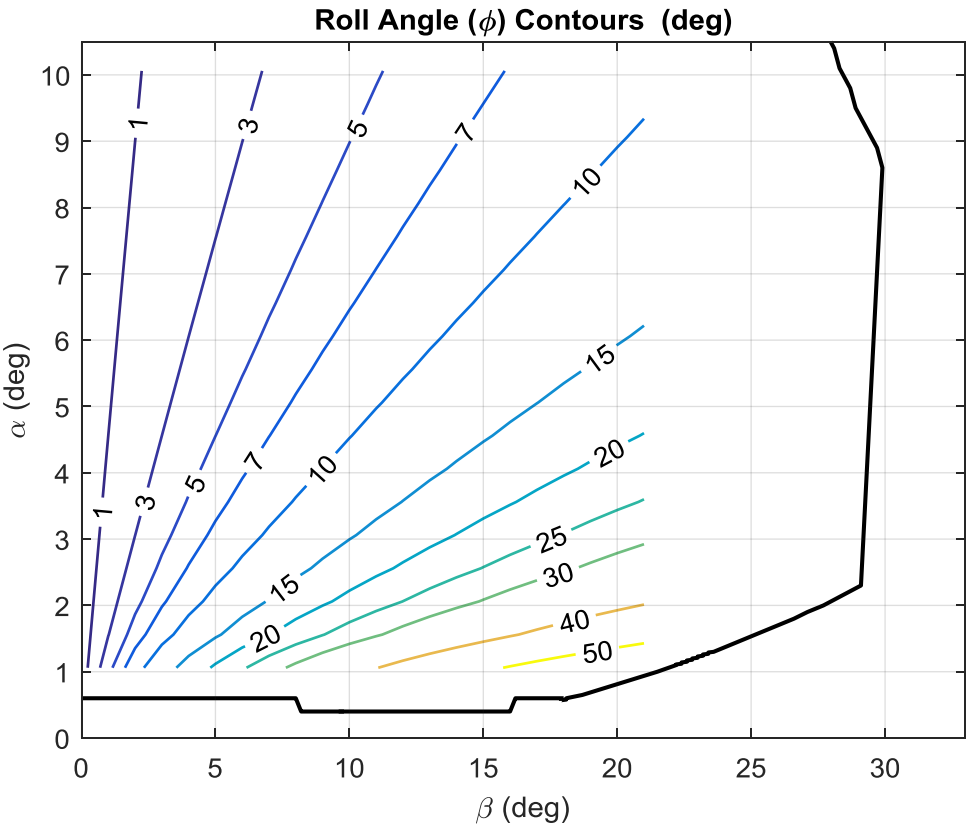

Figure 27: Trim Roll Angle Contours (deg) on a section of α − β Envelope

The variation of elevator deflection (Figure 28) with sideslip angle is similar to that of the military jet model where the elevator deflection is unaffected by change in sideslip angle and only changes with angle of attack. Also, the elevator deflection does not reach its maximum deflection ($\pm 20°$), implying that the lateral controls and thrust play a much bigger role in asymmetric trimming of the aircraft than the elevator.

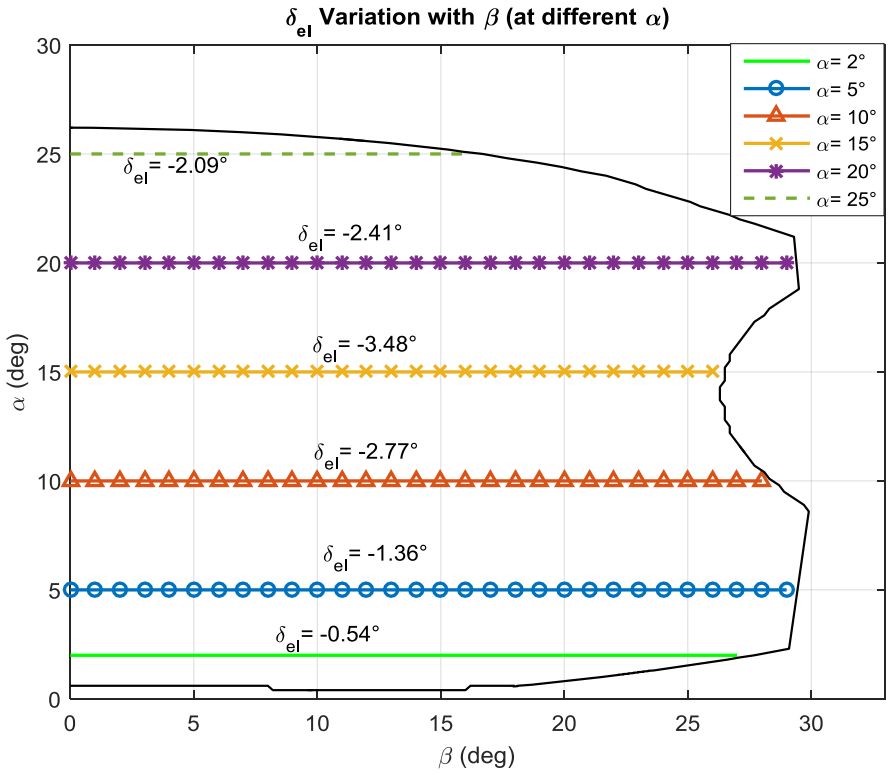

Figure 28: Variation with Sideslip angle of Trim Elevator Deflection at given α values

The variation in trim throttle setting for the business jet model is not presented as contours since the behavior of this control parameter is different than in the military jet model and throttle contours do not offer any noteworthy conclusions here. Figure 29 shows the throttle setting with respect to sideslip angle at various angles of attack ranging from 2° to 25°. The δ_{th} is seen to increase both with angle of attack and sideslip angle, unlike the military jet model, since the thrust is a limiting control parameter for the business jet model. In the figure, for instance, at $\alpha = 2°$ and $\alpha = 25°$, the throttle reaches its 100% maximum setting, which corresponds to its zone of influence in the asymmetric attitude envelope. For angles of attack in the middle of the envelope, the throttle setting is below the maximum. Also, at $\alpha = 2°$, the throttle setting triples from 30% at $\beta = 0°$ to 100% at the envelope boundary. Hence, in the region near the $\bar{q}$-limit, almost all control parameters are affected drastically, for both aircraft models.

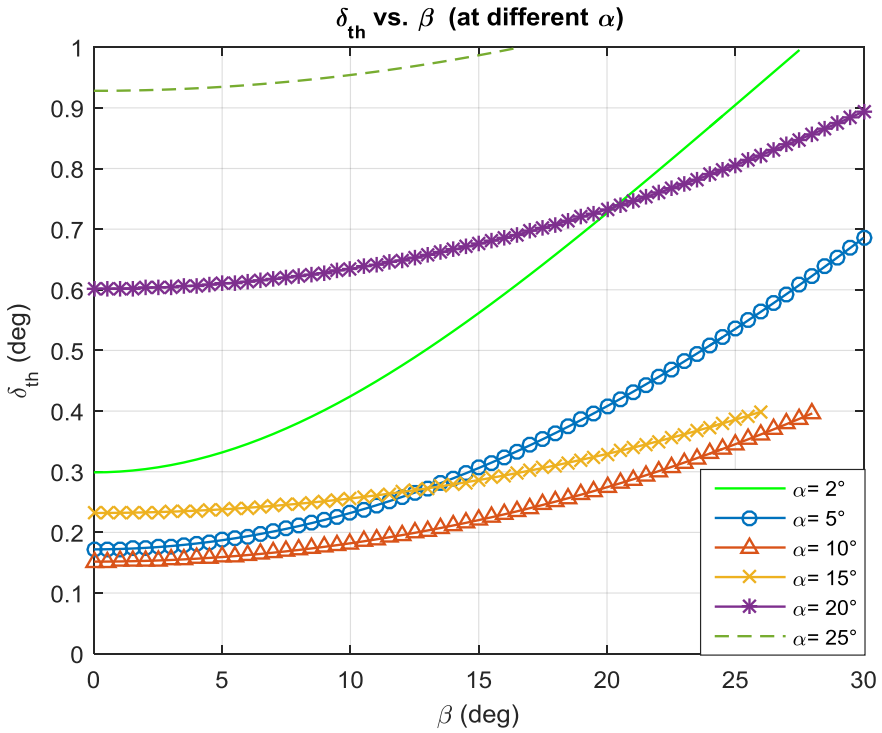

Figure 29: Variation with Sideslip angle of Trim Thrust at given α values

The rudder and aileron deflections are shown in Figure 30 plotted with respect to sideslip angle for angles of attack ranging from $2°$ to $25°$. The rudder and aileron both vary linearly with sideslip angle. However, the rudder deflection is identically linear for all angles of attack. Also, the aileron does reach its maximum deflection of $35°$ within the range of α that lie in its zone of influence. The rudder deflection approaches its maximum deflection ($35°$) but does not reach that value within the asymmetric attitude envelope.

These performance details provide intriguing insights into the trimmability-controllability aspect of flight for both aircraft models.

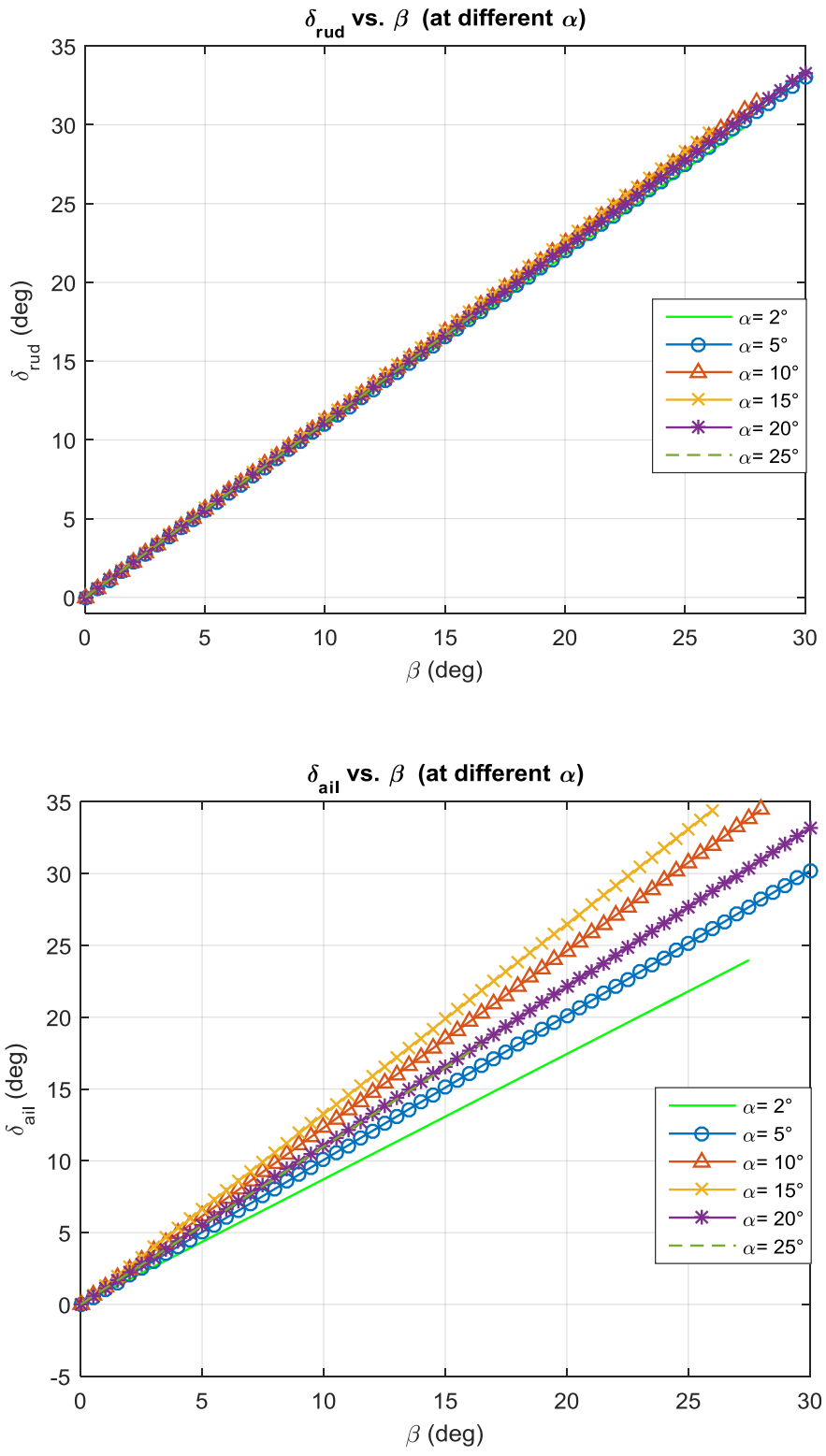

Figure 30: Variation with Sideslip angle of Trim Rudder (top) and Aileron Deflection (bottom) at given α values

The following analysis further remarks on the overall differences and similarities in the envelope characteristics of both aircraft models. It is observed, that the maximum trimmable angle of attack range for the business jet is far below that of the military jet, but the maximum sideslip angle range that can be adopted is higher for the business jet model. However, there are a few caveats to this observation.

Even if such high sideslip and angles of attack combinations are mathematically possible for the business jet, those extreme attitudes are far outside the usual operating conditions required from aircraft with the design mission of the business jet (which is passenger transporting) because there are various external limitations, set by the regulatory authorities, manufacturers and operators of commercial aircraft, about the maximum sideslip and associated bank angle that the aircraft should adopt during normal operation. For instance, passenger and crew comfort factor limits the maximum roll and yaw of civilian aircraft. Also, the allowable aircraft aerodynamic load factor is not the same as fighter aircraft that are designed to sustain high g-force maneuvers frequently, so, flight at extreme attitudes like $25° \alpha$ and $25° \beta$ may have negative effects on the structure of the aircraft.

Additionally, for a fighter aircraft, where the thrust to weight ratio is always close to unity or more, and control surface power and response rate is very high, any extreme attitude possible may be considered relatively feasible (in terms of controllability and stability) because the aircraft can fly trimmed and also potentially recover back to its natural state by utilizing the sheer control power offered by its engine and control surfaces. However, the same cannot be said for civilian aircraft where the thrust to weight ratio is 20-35% only and control power is designed for stability and not high maneuverability, which

dampens the effectiveness and rapid response to pilot control input. Therefore, the feasibility of high sideslip (and coupled bank angle) attitudes may be considered inferior to that of a fighter jet. This trim state feasibility may be studied further in terms of stability analysis of the trim points, which is out of the scope of this work [1],[16].

Regarding the applications of such type of performance assessment methodology, References [9]-[14] describe several applications in the area of aircraft control systems design. As mentioned previously, these systems may consist of offline and online components where the online components which perform real-time calculations, benefit heavily by having considerable offline databases available as data reference, comprising mainly of performance, operational and atmospheric data.

Techniques such as gain scheduling, which utilize multivariable nonlinear data in order to predict and determine the response to an aircraft flight state, make use of such performance data and are present in many adaptive or autonomous flight control systems. These systems can provide real-time maneuverability feasibility and stability augmentation capabilities to an aircraft [9],[13].

The algorithm developed in this work can also be used to simulate and study the effect of asymmetrically damaged components such as airframe panels, segment of wings or tail, etc. Also, the aircraft response for incidents like engine malfunction, control surface hard-overs, jamming or not deflecting fully can be studied by adjusting the aircraft properties and initial conditions of the algorithm. This type of asymmetric damage modeling is scarce in current literature and can aid academic applications [9].

Hence, there is a considerable range and scope of applications, both industrial and academic, of such envelope development methodology and asymmetric flight performance data, in the field of flight dynamics and control.

Finally, it should also be remarked that although the envelope development process has a fixed methodology, the process deviates from this systematic approach at certain stages. This is primarily because this work explores the complete asymmetric trimmablity performance of the respective aircraft models, and such computation over a wide range of attitudes gives rise to unpredictable behavior of the envelope development algorithm. These irregularities affect the envelope results at specific stages and are not readily discernable. This necessitates that full envelope development be carried out with meticulous attention to every detail and parameter involved. As mentioned in Chapter 1, this property of the algorithm requires exhaustive fine tuning and contributes to the cumbersome nature of envelope development.

CHAPTER 7

CONCLUSION

The aim of this work was to develop the asymmetric attitude (α-β) flight envelope for mathematical models of a military and a business jet. This type of flight envelope gives a complete representation of flight performance and acts as an extension to the conventional flight envelopes due to the lack of representation of lateral performance aspects and offers enhanced insights that were not previously available readily. This envelope describes the complete range of aircraft trimmability at asymmetric attitudes of flight.

The requisite governing theory and background were attained through literature review. Certain coefficients for the military jet model were found to have discrepancies and the data was adjusted to reflect the accurate aircraft data from the NASA report. Subsequently, a methodology was established to develop the asymmetric attitude flight envelope, which combined the aircraft aerodynamic models, flight dynamics, propulsive models and the optimization components.

The resulting envelope profiles for the the military jet and the business jet model showed significant differences in trim capabilities and operating limits. The military aircraft had a larger angle of attack envelope profile owing to its design and performance characteristics, and was able to be trimmed at very high angles of attack, while the civilian jet model had a smaller but laterally wider trimmability extent, which was remarked upon and it was concluded that even if numerical trim solution were found at more extreme

sideslip values, these trim points may not be entirely feasible for a civilian jet due to non aircraft performance related factors.

Also, the different control surfaces that were the limiting factors at different zones on the envelope boundary were identified and described. Both the military and the civilian aircraft models were found to have dynamic pressure limit regions at their respective highest-speed regions. The business jet model was also found to have engine thrust limitations in the high-speed region.

Furthermore, using trim data, it was observed that the two aircraft had very different trim requirements at the same points of α and β. The civilian jet never exceeded Mach 0.7 at its highest-speed trim point, while the F-16 reached Mach 1.3. So, even though the two aircraft share a common trim region in the α-β envelope, their trim requirements vary significantly for the same attitudes. This is to be expected as the two aircraft have very different design operating missions and therefore, different aerodynamics and performance requirements.

Additional insights, which are not typically noticeable, were obtained using velocity and roll angle contours, and, the variation of flight control parameters across the asymmetric attitude envelope. These details showed that trim velocity and roll angles were parameters that varied in the same manner in both aircraft models. However, the behavior of the flight control parameters across the envelope were seen to depend on the aircraft model being used.

Hence, the utility and significance of this type of asymmetric attitude flight envelope is evident.

Potential applications of the asymmetric attitude envelope include the development of advanced multivariable flight control techniques such as gain scheduling, adaptive feedback controllers, autopilot and envelope protection controllers, trim state discovery and feasibility, and, analysis of aircraft stability and response. These systems can use the asymmetric attitude performance data as an offline repository of trim and performance parameters and thus perform faster calculations and predictions by interpolating between the various trim states contained within the envelope data, instead of solving large sets of equations in real-time.

Recommendation for future work include increasing the degree of automation of the envelope development algorithm since there exist sensitivities within the algorithm that make the process quasi-automated, as discussed formerly. Another recommendation for future work would cover a thorough stability analysis of asymmetric trim performance data which may be carried out for both aircraft models to discover the regions where trim points are stable and where the instabilities lie.

References

[1] Abdallah, A. M., Newman, B. A., & Omran, A. M. (2013). Measuring Aircraft Nonlinearity Across Aerodynamic Attitude Flight Envelope. AIAA Atmospheric Flight Mechanics (AFM) Conference. doi:10.2514/6.2013-4985

[2] Abdallah, A. M., Newman, B. A., & Omran, A. M. (2014). Measuring Aircraft Nonlinearity Across Aerodynamic Attitude Flight Envelope-Revisited With Symmetrized Aerodynamics. AIAA Atmospheric Flight Mechanics Conference. doi:10.2514/6.2014-2193

[3] Abdallah, A. M. (2018). A New Concept for Three-Dimensional Aerodynamic Attitude Flight Envelope. 2018 Atmospheric Flight Mechanics Conference. doi:10.2514/6.2018-3153

[4] Admin. (2019, March 15). Aircraft Load Diagram - 19.7.kenmo-lp.de •. Retrieved March 17, 2019, from http://19.7.kenmo-lp.de/aircraft_load_diagram.php

[5] Cessna Citation Mustang. (2019, March 26). Retrieved from https://en.wikipedia.org/wiki/Cessna_Citation_Mustang

[6] General Dynamics F-16 Fighting Falcon. (2019, March 27). Retrieved from https://en.wikipedia.org/wiki/General_Dynamics_F-16_Fighting_Falcon

[7] Filippone, A. (2006). *Flight performance of fixed and rotary wing aircraft*. Amsterdam: Elsevier Butterworth-Heinemann.

[8] Marco, A. D., Duke, E., & Berndt, J. (2007). A General Solution to the Aircraft Trim Problem. AIAA Modeling and Simulation Technologies Conference and Exhibit. doi:10.2514/6.2007-6703

[9] Nabi, H. N., Lombaerts, T., Zhang, Y., Kampen, E. V., Chu, Q. P., & Visser, C. C. (2018). Effects of Structural Failure on the Safe Flight Envelope of Aircraft. *Journal of Guidance, Control, and Dynamics, 41*(6), 1257-1275. doi:10.2514/1.g003184

[10] Nelson, R. C. (1989). Flight stability and automatic control. New York: McGraw-Hill.

[11] Nguyen, L. T., Ogburn, M. E., Gilbert, W. P., Kibler, K. S., Brown, P. W., & Deal, P. L. (1979). simulator study of stall/post-stall characteristics of a fighter airplane with relaxed longitudinal static stability. NASA Technical Paper, (1538)

[12] National Programme on Technology Enhanced Learning. (n.d.). Retrieved March 28, 2019, from https://nptel.ac.in/courses/101104007/Module6/Lec26.pdf
6 DOF equations of motion

[13] Stengel, R. F. (2004). Flight dynamics. Princeton, NJ: Princeton University Press.

[14] Stevens, B. L., & Lewis, F. L. (2003). Aircraft control and simulation. Hoboken, NJ: J. Wiley.

[15] Stinton, D. (1998). The Anatomy of the airplane. Reston, VA: American Institute of Aeronautics and Astronautics.

[16] Yi, G., Zhong, J., Atkins, E. M., & Wang, C. (2015). Trim State Discovery with Physical Constraints. Journal of Aircraft, 52(1), 90-106. doi:10.2514/1.c032619

Vitae

Name	: Mohammed Abdul Muqeeth
Nationality	: Indian
Date of Birth	:2/26/1993
Email	: mqth1234@gmail.com
Address	: House # 16/2/51/10/1, Akbarbagh, New Malakpet, Hyderabad, Telangana 500036, India
Academic Background	: MS in Aerospace Engineering from KFUPM in 2018 BS in Aerospace Engineering from KFUPM in 2015